Co-infection with *Toxoplasma gondii* leads to a loss of resistance in *Heligmosomoides bakeri* trickle-infected mice due to ineffective granulomas

Breton Fougere[1,2*], Anupama Ariyaratne[1,2*], Naomi Chege[1,2], Shashini Perera[1,2], Emma Forrester[1,2], Mayara de Cassia Luzzi[1,2], Joel Bowron[1,2], Aralia Leon Coria[1,2], Edina Szabo[1,2], Constance A. M. Finney[1,2]

[1]Department of Biological Sciences, Faculty of Science, University of Calgary, Calgary, Alberta, Canada.

[2]Host-Parasite Interactions Research Training Network, University of Calgary, Calgary, Alberta, Canada.

*Co-authors

Corresponding Author: Constance A. M. Finney, constance.finney@ucalgary.ca, Faculty of Science, Department of Biological Sciences, University of Calgary, 2500 University Drive N.W., Calgary, Alberta, Canada.

Keywords: parasitic worm infections, Toxoplasma, nematodes, granuloma, innate immunity, antibody responses, trickle infection, co-infection

ABSTRACT

The intestinal roundworm *Heligmosomoides bakeri* causes chronic infection in susceptible (C57Bl/6) mice; however, repeat (trickle) infection confers immunity and facilitates worm clearance. We previously showed that this acquired immunity is associated with a strong Th2 response, notably the enhanced production of intestinal granulomas. Here we demonstrate that elevated proportions of IgG_1-bound eosinophils and macrophages are observed around the developing tissue worms of trickle-infected female C57Bl/6 mice compared to bolus infected animals. Levels of IgG_{2c}, IgA or IgE were not detected in the granulomas. Increased proportions of $SiglecF^+$ and $CD206^+$ cells, but not $Ly6G^+$ and/or $NK1.1^+$ cells, were also found in the granulomas of trickle-infected mice. However, in the natural world rather than the laboratory setting, immune environments are more nuanced. We examined the impact of a mixed immune environment on trickle infection-induced immunity, using a pre-infection with *Toxoplasma gondii*. The mixed immune environment resulted in fewer and smaller granulomas with a lack of IgG_1-bound cells as well as reduced proportions of $SiglecF^+$ and $CD206^+$ cells, measured by immunofluorescence and flow cytometry. This was associated with a higher worm burden in the co-infected animals. Our data confirm the importance of intestinal granulomas and parasite-specific antibody for parasite clearance. They highlight why it may be more difficult to clear worms in the field than in the laboratory.

AUTHOR'S SUMMARY

Despite decades of research on intestinal parasitic worms, we are still unable to clearly point to why so many people (approximately 1.8 billion) and most livestock/wild animals are infected with these parasites. We have made progress in understanding how the immune system responds to parasitic worms, and how these parasites manipulate our immune system. However, identifying effective clearance mechanisms is complex and context dependent. We have used models of trickle infection (multiple low doses of parasites) and co-infection (two intestinal parasites) to simulate how people/animals get infected in the real world. Using these models, we have confirmed the host/parasite interface (the granuloma) within the intestinal tissue to be key in determining the host's ability to clear worms. The lack of specific immune cells and antibodies within the granuloma was associated with chronic infection. Our results help explain why intestinal parasitic worms are so prevalent and why it may be difficult to clear worms in natural settings.

INTRODUCTION

Gastrointestinal nematodes (GINs) are ubiquitous. They are highly prevalent in humans [1], livestock (reviewed in [2]) and pets [3]. Despite the low mortality associated with these parasites, they significantly impact human and animal health (reviewed in [4–6]). Infected hosts mount strong anti-GIN immune responses, but the efficacy of the response is dependent on genetics, infection dynamics and the environment, and we have yet to find treatments that clear worms and prevent reinfection. Understanding effective clearance mechanisms by the host in natural settings is key to developing strategies to stimulate sterile immunity.

Heligmosomoides bakeri (Hb), formerly *Heligmosomoides polygyrus* [7], is a rodent model gastrointestinal nematode parasite which has been extensively used to understand host/parasite interactions in related livestock and human parasites [8]. For the first 7-10 days of infection, Hb develops within the tissue. After 10 days, adults emerge into the lumen, where they remain coiled around the intestinal villi for the duration of infection. Hb infection stimulates a strong Th2 response, ultimately dependant on the production of IL-4 and IL-13, and IL-4 receptor signalling for effective clearance [9,10]. Tissue dwelling parasite stages induce an influx of immune cells to the site of infection culminating in the formation of an intestinal granuloma (reviewed in [11]). The levels of IL-4/IL-13, and the size and number of granulomas are associated with the resistant/susceptibility phenotype of different mouse strains [12,13].

Immune protection from reinfection, observed in laboratory models of vaccination and/or secondary infections, has been linked to effective immune responses against tissue dwelling Hb stages [14–16]. Within the granuloma, the host response simultaneously immobilises, damages and/or kills the parasites while healing the damage caused by the growing worm (reviewed in [11]). Due to their size, parasitic worms cannot be phagocytosed by immune cells; antibody-bound myeloid cells, namely SiglecF+ eosinophils and CD206+ macrophages, within the granuloma have been implicated in protection (reviewed in [11]).

Resistant strains of mice develop faster and stronger parasite-specific antibody responses to Hb, as compared to susceptible strains [12,13]. More specifically, elevated levels of IgG_1, IgA and IgE have been linked to worm clearance [17–20]. Passive transfer of serum, more specifically IgG_1, from infected mice decreases adult worm numbers as well as their fitness [21–24]. Mice lacking IgG, and to a lesser extent IgA, but not IgE, have increased worm burdens upon secondary infection compared to wild-type animals [18]. In support of this, macrophages isolated from Hb-induced granulomas from challenge infected mice are bound to IgG isotypes (IgG_1 and IgG_3) but not IgE [15]. They also express high levels of FcγRs, and mice lacking FcγRs (unable to bind IgG antibodies) have increased parasite loads [16].

102 While it's clear that in the context of a Th2 immune environment generated in a
103 laboratory-based experimental model, susceptible strains of mice can mount strong
104 immune responses to reinfections with Hb [13,18], in natural settings, where immune
105 environments are more nuanced, Hb prevalence is high [25–27]. One of the many factors
106 that influence immune environments is co-infection, a common occurrence in the
107 natural world [28].
108
109 The overarching aim of our study was to examine the impact a mixed immune response
110 on effective clearance of Hb. As an obligate intracellular parasite, *Toxoplasma gondii*
111 (Tg) elicits a strong inflammatory response in the small intestine during infection, with
112 elevated IL-12 and IFNγ levels (as reviewed in [29]). Following infection of the intestinal
113 mucosa, IL-12 producing monocytes and neutrophils are recruited to the small intestine,
114 where they recruit ILC1s and T cells, both potent producers of IFNγ. Research suggests
115 that previous Tg infection skews Hb-specific $CD4^+$ T cell and IgG antibody responses
116 towards a more Th1 phenotype, with no impact on worm burden [30]. However, this
117 previous study focused on a primary chronic infection (28 days post infection - D28) and
118 did not address potential impacts to the host/parasite interface in the granuloma. We
119 used the more realistic trickle model of TgHb confection and show that TgHb infected
120 animals have a reduction in the size and number of granulomas, and that their
121 granulomas have fewer myeloid cells and more specifically, IgG_1-bound myeloid cells.
122 The lack of functional granulomas was associated with increased worm burdens. Our

data confirm the importance of intestinal granulomas in the context of re-infection, and highlight why it may be more difficult to clear worms in the field than in the laboratory.

MATERIALS AND METHODS

Mice, Parasites and Antigens

Female BALB/c and C57Bl/6 mice aged 6-10 weeks were bred and maintained in the Life and Environmental Science Animal Resource Centre (LESARC) in the Department of Biological Sciences, University of Calgary, Canada. Original stocks were obtained from Charles River, Canada. Mice were acclimatised for a minimum of two days when moved to our experimental room and housed in groups of 3-5 in individually vented cages. All experiments were approved under protocol # AC17-0083 and AC19-0121 by the University of Calgary's Life and Environmental Sciences Animal Care Committee. All protocols for animal use and euthanasia were in accordance with the Canadian Council for Animal Care (Canada). Enrichment was provided in the form of plastic housing, bedding and for parasite passage animals, a variety of veterinary approved small treats (seeds, nuts, etc) and/or supportive nutrition (DietGel).

Mice were orally infected by gavage with 200 third stage *Heligmosomoides bakeri* larvae (maintained in house, stock was a gift from Dr. Allen Shostak, University of Alberta, Canada and Dr Lisa Reynolds, University of Victoria, Canada) and euthanized at either

145 D5, D7, D21 or D28. Larvae were obtained from fecal cultures after approximately 8-9
146 days of incubation at room temperature. Mice were infected according to the bolus or
147 trickle infection regimes (Figures 1A & 4A). To avoid differences in counts during the
148 trickle infections, on D0, two identical solutions were made up (200 worms/100µl). One
149 was used to infect the bolus infected mice on D0 and one was used for the trickle-
150 infected mice. The solution for the trickle-infected animals was divided into ten equal
151 parts. Each part was made up to 100ul using water. Animals were gavaged with a diluted
152 solution on days 0, 2, 4, 6, 8, 10, 12, 14, 16 and 18. Using the 10 doses, trickle-infected
153 animals received 200 larvae in total over 18 days.
154
155 The Me49 strain of *Toxoplasma gondii* (Tg) (maintained in house, original stock was a
156 gift from Dr. Georgia Perona Wright, University of British Columbia, Canada) was
157 maintained in male C57BL/6 and CD1 mice by alternating bimonthly passage into new
158 animals. Cysts were obtained from the brains of these animals a month after infection.
159 Ten cysts were orally administered per mouse (female C57BL/6) followed by Hb larvae
160 14 days later. Mice were euthanized 21 or 28 days post Hb infection (Fig 7A).
161
162 Sample size was calculated based on numbers used in our previous work [13] or for the
163 flow cytometry of granuloma cells, on infecting enough animals to obtain the required
164 amount of cells. No animals for which we obtained data were excluded from analysis.
165 However, criteria had been set. We would have excluded all animals developing
166 pathologies unrelated to infections during the experiment or observed during necropsy

167 (e.g. tumours). Animals were not randomised. Co-infections and trickle infections
168 require many manipulations. Our experience is that using confounders increases
169 mistakenly providing the incorrect treatment to the mice.
170
171 All mice were monitored daily. Humane endpoints were defined as: general decline of
172 health, respiratory distress, severe neurological signs, loss of body weight > 20% or
173 recommendation from the facility veterinarian. Animals were euthanised within 24
174 hours of humane endpoints being observed. For TgHb animals, a small number of
175 animals were found dead before the 28 days post-Hb infection. This happened towards
176 the end of the experiment, usually in the early morning, after a check of humane
177 endpoints the previous day.
178
179 Hb antigen was prepared by collecting live adult worms from 14/21 or 28-day infected
180 mice using modified Baerman's apparatus. Worms were washed multiple times and
181 homogenized in PBS using a glass homogenizer. The resulting solution was centrifuged
182 (13, 000 g, 10 minutes, 4°C) and the supernatant filtered (0.2mm filter, Nalgene). The
183 protein concentration was calculated using the Bradford assay. The antigen was stored
184 at 15 mg/ml at -80°C.
185
186 We collected immune serum from trickle infected mice euthanized at D14 using a
187 previously published trickle infection model [13]. We transferred 100ul intravenously to
188 bolus infected mice at day 0, day 2, day 4 and day 6.

Worm and Granuloma Counts

Small intestines of infected mice were harvested and opened longitudinally. The number of adult worms present in the intestinal lumen along the length of the small intestine was counted under a dissection microscope. Macroscopic granulomas were counted by eye under a dissection microscope with the small intestine intact.

Granuloma size

Consecutive formalin fixed paraffin embedded mouse small intestinal sections were stained with H & E by the University of Calgary's Veterinary Diagnostic Services Unit. Stained tissue sections were analyzed visually using the Leica DMRB light microscope and/or the OLMYPUS SZX10 microscope. Images of granuloma were captured using the QCapture and the cellSens software and processed using the ImageJ software, in a blinded manner. Whole granuloma and necrotic centre size were measured for each granuloma on the slide. Granuloma area was calculated using ImageJ. Granuloma were outlined using the freehand perimeter tool and area was calculated using a pre-determined measurement scale.

Serum ELISAs

211 Blood samples were left to clot for 30 minutes and then centrifuged twice at 11, 000 g at
212 4°C for 10 minutes. Serum was collected and used either fresh or stored at -80°C. Total
213 IgE (BD, 555248) and IgA (capture antibody, BD, 556969, detection antibody, BD,
214 556978) and IgG1 levels (capture antibody, BD, 553440, detection antibody, BD,
215 553441) were measured by ELISA according to manufacturer's instructions.
216
217 Antigen specific antibody responses were also measured by ELISA. ELISA microplates
218 were coated with 10 mg/ml *H. bakeri* antigen in carbonate buffer (0.1mM NaHCO3, pH
219 9.6), overnight at 4°C. Plates were blocked with 2% BSA in TBS/ 0.05% tween 20 for 2
220 hours at 37°C. Sera were diluted in TBS Tween and added to wells overnight at 4°C.
221 Antigen-specific IgG1 was detected with HRP-conjugated corresponding detection
222 antibodies (anti-IgG1, BD, 553441) with TMB peroxidase substrate (T3405, Sigma). The
223 reaction was stopped using 1M H2SO4 solution and the color change was read at
224 450nm.
225
226 Intestinal tissue homogenate ELISAs
227
228 Small intestines were opened longitudinally and washed with PBS to remove luminal
229 content. The mucosal surface was identified under a dissecting microscope. The mucosal
230 surface (with its mucus) was gently scraped using a glass slide. Scrapings were weighed,
231 added to 500 ml lysis buffer (10 mM tris HCl, 0.025% sodium azide, 1% tween 80, 0.02%
232 phenylmethylsulfonyl fluoride) with one complete protease inhibitor tablet (Roche

233 diagnostics GmbH, Germany) and homogenized using a bead beater (40 seconds at
234 speed 6 using the Fast-prep-24 bead beater, MP biomedical). The homogenate was
235 centrifuged at 11, 000 g at 4°C for one hour. Supernatants were collected and used fresh
236 or stored at -80°C. IgA (IgA (capture antibody, BD 556969, detection antibody, BD
237 556978), IL-4 (R & D systems, DY404 kit), IL-13 (R & D systems, DY413 kit) and IL-21 (R &
238 D systems, DY594 kit) was measured by ELISA according to manufacturer's guidelines.
239 All IL-21 ELISAs were performed on fresh, unfrozen material [31].
240
241 MLN and SPL Cell isolation, *in vitro* re-stimulation assay and cytokine ELISAs
242
243 Mesenteric lymph nodes (MLN) and spleens (SPL) were mechanically dissociated into
244 single cell suspensions. Cells were counted using a Beckman-Coulter ViCell XR. MLN and
245 SPL were cultured at 1 x 10^6 cells/ml for 48 hours in RPMI medium, 10% FCS, 1% L-
246 glutamine, 1% penicillin/ streptomycin (supplemented RPMI 1640) in the presence of 10
247 mg/ml *H. bakeri* antigen or 2 mg/ml concanavalin A (Sigma) at 37°C with 5% CO2.
248 Supernatants were collected for cytokine measurements. Measurements for antigen-
249 specific production were not included in the analysis unless cytokine production was
250 observed in the wells with concanavalin A stimulation. ELISAs were performed according
251 to manufacturer's guidelines (R & D systems, DY404 kit for IL-4 and DY413 kit for IL-13).
252
253 Transit time
254

255 Gastrointestinal transit time was measured one day prior to euthanasia. Mice were
256 fasted for 6 hours and 200 ml of 5% Evans blue (Sigma) in 5% gum arabic (ACROS
257 organics) was orally gavaged using a ball tip 20 gauge 1.5'', 2.25mm curved animal
258 feeding needle. Each mouse was labelled, with the time of dye administration recorded.
259 Mice were transferred to clean empty cages and the time to pass the first blue fecal
260 pellet was recorded. Gastrointestinal transit time was calculated for each mouse.
261
262 Immunofluorescence
263
264 Whole small intestines were fixed in formalin for a minimum of 48 hours, washed in
265 saline for a minimum of 48 hrs and processed to obtain paraffin embedded tissue
266 blocks. 6um sections were cut by the Diagnostic Services Unit, UCalgary. The sections
267 were stained for H&E or with either anti-mouse IgG_1 (BD 562026), anti-mouse IgA (BD
268 559354), anti-mouse IgE (BD 553415), anti-mouse IgG_{2c} (Invitrogen SA5-10221) or their
269 respective isotypes overnight at 4°C. Slides were mounted with FluoroshieldTM with
270 DAPI (Sigma-Aldrich F6057). Images were acquired using the Zeiss Axio ZoomV.16
271 stereoscopic microscope (Bio Core Facility, University of Calgary) or the Thorlabs Tide
272 whole- slide scanning microscope (Live cell imaging Facility, University of Calgary).
273 Brightfield and fluorescence images were taken either under the 2.3x objective with the
274 AxioCam High Resolution color (HRc) and High-Resolution mono (HRm) cameras, or the
275 20x/0.75 NA objective of the slidescanner respectively. Zeiss Zen (blue edition) software
276 or Thorlabs Tide LS image acquisition software was used. DAPI, FITC and Texas Red

277 fluorophores were used. Brightness and contrast were adjusted similarly for all
278 photographs in photoshop.
279
280 Granuloma Digestion for Flow cytometry
281
282 Granulomas were identified along the small intestine as tissue (containing worms) or
283 lumen (chronic granuloma not containing worms) using a dissection microscope.
284 Granulomas from 5 mice were pooled by infection type (trickle/bolus/co-infected) and
285 granuloma type (tissue/lumen). Isolated granulomas were incubated with DNAse (Roche
286 10104159001) and 1:50 Liberase (Roche 0540102001)) at 37°C for 90 minutes. After
287 incubation, granulomas filtered, washed, centrifuged and stored at 4°C until use.
288 Cells were counted using a Vi-CELLTM XR Cell Analyzer (Beckman Coulter 731196). $1x10^6$
289 cells (100µL) were used per sample. Samples were stained with fixable viability stain
290 (BD, 565388 or BD 564406) for 15 minutes at RT in dark, blocked with rat anti-mouse
291 CD16/32 (BD 553142) for 5 minutes at 4°C in the dark and stained for surface markers
292 for 20 minutes at 4°C in the dark. For the granuloma panel, cells were stained for CD3
293 (BD 560591), CD19 (BD 612781), NK1.1 (BD 564143), SiglecF (BD 552126), CD206 (BD
294 565250), Ly6G (BD 740953), CD11b (BD 563553), and IgG1 (BD 553443).
295
296 For intracellular staining (IgG_1 and IgA), samples were fixed, permeabilized and stained
297 for IgG_1 (BD 553443) and IgA (BD 743293) or isotype controls (BD 554684, BD 562868)
298 for 30 minutes at 4°C. Samples were then washed and centrifuged. Resuspended

samples were run on an LSRFortessaTM X20 (BD Biosciences) flow cytometer. Data was acquired using FACSDivaTM software, and analysis of cell populations was performed using FlowJoTM software (v10.7.1).

MLN and Peyer's Patches Isolation for Flow Cytometry.

Peyer's patches (PP) and MLN were removed from the small intestine under the dissection microscope. Cells were mechanically dissociated into single cell suspensions. PP and MLN cells were counted using a Vi-CELLTM XR Cell Analyzer (Beckman Coulter 731196). $1x10^6$ cells (100µL) were used per sample. Samples were stained with fixable viability stain (BD 564406) for 15 minutes at RT in dark, blocked with rat anti-mouse CD16/32 (BD 553142) for 5 minutes at 4°C in the dark and stained for surface markers for 20 minutes at 4°C in the dark. For the plasma cell panel, cells were stained for CD3 (BD 566495), IgD (BD 558597), B220 (BD 561880), CD19 (BD 612781), and CD138 (BD 563193/565176).

RNA/DNA Extraction and Quantitative PCR

RNA and gDNA were extracted from 4 equal snap frozen sections of the SI (sections 1-4, where 1 is the most proximal section and 4 the most distal from the stomach) by crushing the tissue in Trizol (Ambion, Life Technologies) using a pestle and mortar on dry ice. We followed manufacturer guidelines for RNA extraction. To measure cytokine

321 levels in the RNA samples, cDNA was prepared using DNase 1 (RNase-free, New England
322 Biolabs), and iScript Reverse Transcription Supermix for RT-qPCR (Bio-Rad) or
323 AdvanTech 5x Revese Transcription master mix (Diamed).
324
325 Primers for quantitative PCR were obtained from Integrated DNA Technologies (San
326 Diego) for IL-13 (GATCTGTGTCTCTCCCTCTGA forward, GTCCACACTCCATACCATGC
327 reverse), IFNγ (TCAAGTGGCATAGATGTGGAAGAA forward, TGGCTCTGCAGGATTTTCATG
328 reverse), IL-10 (GTCATCGATTTCTCCCCTGTG forward, ATGGCCTTGTAGACACCTTG
329 reverse) and 18S rRNA (GCAATTATTCCCCATGAACG forward, GGCCTCACTAAACCATCCAA
330 reverse). Samples were run in triplicate on a Bio-Rad CFX96 real time system C1000
331 touch thermocycler. Relative quantification of the cytokine genes of interest was
332 measured with the delta-delta cycle threshold quantification method [32], with 18S rRNA
333 for normalization. Data are expressed as a fold change relative to 18S rRNA levels for
334 each animal.
335
336 ELIspot Assay
337
338 Plates were then coated with either purified rat-anti mouse IgG1 (BD 553440) or Hb
339 antigen and incubated overnight at 4°C. Plates were washed and blocked with media for
340 2 hours at 37°C with 5% CO_2. MLN cells added in triplicate at $5x10^3$ cells/mL to measure
341 total IgG1 producing cells. For quantifying *H. bakeri* antigen-specific IgG1 producing
342 cells, a total of $2x10^6$ cells were cultured overnight at 37°C with 5% CO_2. For detection,

IgG1 (BD 553441) was incubated for 2 hours at RT, followed by a Streptavidin-HRP (horseradish peroxidase; BD 554066) incubation for 1 hour at RT. Spots were allowed to develop for 5-7 minutes once the substrate solution had been added, before stopping the reaction. Plates were allowed to dry for 24-48 hours, before spots were counted manually under a dissecting microscope.

Statistical Analysis

Graphpad Prism software (La Jolla, CA, USA) was used for all statistical analysis. To compare multiple groups (three or more), we performed a normality test (D'Agostino and Pearson test, unless N too small, in which case Anderson-Darling or Shapiro-Wilk). ANOVA or Kruskal-Wallis tests were performed on parametric/non-parametric pooled data, and when significant, Sidak's/Dunn's Multiple comparisons were performed on Hb vs. HbTg and Tg vs. HbTg. For comparisons of 2 groups, statistical significance was assessed by either an unpaired t test (for data sets with normally distributed data) or Mann-Whitney's U test (for non-parametric data) or paired t test (for paired data sets with normally distributed data). Data are presented as median and individual data points, unless otherwise specified.

RESULTS

364 ***The resistant phenotype in trickle infected C57Bl/6 mice is not associated with***
365 ***increased Th2 cytokine or antibody levels.***
366
367 We have previously shown that using a trickle regimen, C57Bl/6 mice harbour fewer Hb
368 worms and have more granulomas than bolus infected mice [13]. Using a more robust
369 trickle model (more doses and later time points, Fig. 1A), we show even starker
370 differences depending on the mode of infection. After 28 days (D28), the Hb worm
371 burden (primary outcome) of the trickle-infected group was below 5 worms in 8/10
372 animals compared to a mean of 76 in bolus infected animals (Fig 1B). The granuloma
373 number was also higher in trickle infected animals, with 9/10 mice having more
374 granulomas than the bolus infected mouse with the most granulomas (32 granulomas,
375 Fig. 1C). Despite granuloma size being associated with susceptibility/resistance
376 phenotypes [12], we found that this parameter was not affected by the mode of infection.
377 Neither the size of the whole granuloma, nor the size of the internal necrotic centre
378 changed with the mode of infection (Fig 1D and 1E). However, as we have previously
379 shown with trickle infection [13], granuloma composition differs between bolus and trickle
380 infected animals. Macrophages numbers are similar (Fig 1F) but eosinophil numbers are
381 increased (Fig 1G). In resistant Balb/c animals, we see no differences in worm burden or
382 granuloma number between bolus and trickle infected animals (Sup Fig 1A and 1B).
383
384 A strong Th2 response is responsible for anti-parasitic worm immunity. Increased levels
385 of IL-4 and IL-13 in the MLN (mesenteric lymph nodes) and SPL (spleen) are commonly

386 reported in bolus infected animals and have been directly linked to parasite
387 clearance[9,10,33–35]. However, in trickle infected animals, previous studies have not linked
388 reduced parasite burdens to an increase in these cytokines [13,36]. We found no
389 differences in the levels of IL-4 and/or IL-13 between bolus and trickle infected mice,
390 apart from IL-13 in the SPL (Fig 2A-F). SPL IL-13 levels were recorded per cell and likely
391 decreased in the trickle infected animals in response to the low worm burden. When
392 accounting for differences in total cell number (Fig 2E and 2F), IL-4 and IL-13 levels in the
393 MLN and SPL in trickle and bolus infected animals remain similar. Levels of IL-4 and IL-13
394 were undetectable in the serum, as previously observed [13]. Again, in resistant Balb/c
395 animals, we see no differences between bolus and trickle infected animals in any of the
396 parameters measured, apart from spleen IL-13 (Sup Fig 1C-H).
397
398 Th2 immune responses can also be observed closer to the host/parasite interface, in the
399 Peyer's patches (PP) and the small intestine (SI). Levels of the Hb antigen-specific IL-4
400 and IL-13 were again similar between bolus and trickle infected animals (Fig 2G-J). No
401 levels of IL-5, IL-9 or IL-10 were detectable in intestinal tissue from control or infected
402 mice, as previously observed [13]. Increased mucus production [37], intestinal smooth
403 muscle contractility [38] and IL-21 levels [39] have all been associated with parasite
404 clearance. However, none of these parameters differed between the two infected
405 groups in the SI (Fig. 2K-M).
406

407 Resistance to Hb has also been linked to increased parasite-specific IgG_1, IgA and IgE
408 levels [18]. Total IgG_1 and IgE levels were increased in the serum of infected vs. naïve mice
409 (Fig 3A and 3B). However, the levels did not change with the mode of infection. No
410 difference was observed in the levels of parasite specific IgG_1 either (Fig 3C). Levels of
411 intestinal IgA did not differ between naïve, bolus infected or trickle infected animals (Fig
412 3D). No detectable levels of Hb larval or adult parasite antigen specific IgE, IgG_{2c} or IgA
413 were observed in the serum of bolus- or trickle-infected mice. In resistant Balb/c
414 animals, we see no differences between bolus and trickle infected animals in IgE or IgG_1
415 levels (Sup Fig 1I-K).
416
417 By D28 of infection, all worms had migrated from the tissue to the lumen. Our results
418 are therefore unsurprising in light of the importance of immunity against developing
419 tissue parasite stages, which are best observed at the host/parasite interface early
420 during infection. We next focused our efforts on studying immune responses within the
421 granuloma during acute infection.
422
423 ***Cell-bound IgG_1 antibodies accumulate around encysted larvae in the granulomas of***
424 ***trickle-infected C57Bl/6 mice.***
425
426 By D10 most, if not all, parasites have matured into adults, and left the tissue to inhabit
427 the lumen. Previous research has demonstrated that the resistance to Hb attained by
428 the host after vaccination and/or secondary infection is aimed at incoming larvae [14,15].

429 To study immune responses against larvae in the trickle infected animals, we euthanised
430 mice at D21 instead of D28 (3 instead of 10 days after the final parasite dose). This
431 ensured there were both developing parasites in the tissue and adults in the lumen. We
432 matched these to an early (D5) and late (D21) bolus infection (Fig 4A).
433
434 Tissue dwelling stages are immobilised/damaged/destroyed by antibody-bound cells
435 within the granulomas (reviewed in [11]). To quantify antibody levels within granulomas,
436 we isolated worm containing (acute) and non-worm containing (chronic) granulomas
437 and measured antibody levels on the isolated cells by flow cytometry (Sup Fig 2 for
438 gating strategy). Acute granulomas from trickle infected animals had the highest levels
439 of $CD11b^{+}IgG_1^{+}$ cells (Fig 4B and 4C). We confirmed these findings by staining for
440 antibodies in intestinal tissue sections isolated from infected mice (Fig 4D-F).
441 Interestingly, we only detected IgG_1 within the acute granulomas, and did not observe
442 any IgG_{2c} (Fig 2E), which has previously been linked to trapping developing worms
443 within granulomas upon secondary infection [15]. We did not observe IgA or IgE (Fig 2F)
444 within the granulomas either, confirming that IgG_1 is the key antibody subtype
445 associated with resistance in our model. Our results are in accordance with previous
446 work studying vaccination mediated protection [14].
447
448 Chronic granulomas had very low/background levels of IgG_1 (Fig 4G-I). However, despite
449 this, the granulomas from trickle infected animals were bigger (Fig 4J), with necrotic
450 centres of similar size (Fig 4K). Since this difference was not apparent at D28, the

451 observation is likely due to granuloma age. Once the worms have left the granulomas
452 and/or been killed within it, granulomas resorb. Chronic granulomas in the bolus
453 infected animals are all ~18 days old (granulomas start forming within 3 days of
454 infection), those in the trickle infected animals range in age from 8-18 days.
455
456 To assess whether the differences in granuloma antibody levels were due to differences
457 in antibody production, we measured plasma cell antibody levels at D21 in the MLN and
458 PP, the closest antibody-producing sites to the granulomas (Fig 5, Sup Fig 3 for gating
459 strategy). Plasma cell percentages in the MLN and PP of trickle infected mice were
460 decreased compared to bolus-infected mice; their numbers in the MLN followed this
461 trend (Fig 5A-D). We focused on IgA and IgG_1 levels because previous work has
462 demonstrated that, in a secondary infection, animals lacking these antibodies have
463 higher worm burden than wildtype animals [18]. At D21, intracellular IgG_1^+ plasma cell
464 percentages in the MLN (Fig 5E) and PP (Fig 5F) in trickle infected mice were increased
465 compared to naïve animals but decreased compared to bolus infected animals. Cell
466 numbers in the MLN followed this trend (Fig 5G). As expected, percentages in the MLN
467 were far greater than in the PP [18]. The decrease could be attributed to a lack of parasite
468 stimulation in the trickle infected animals, which have significantly lower worm burdens.
469 No differences were found between trickle and bolus infected animals with regards to
470 IgA^+ plasma cell percentages and/or numbers in the MLN and/or PP (Fig 5I-K). The
471 amount of soluble antibody produced per cell, measured by mean fluorescence index

472 (MFI) ratios, did not differ for either the antibody type (IgG_1 or IgA) or the immune site
473 (MLN or PP) between bolus and trickle infected mice (Fig 5L-O).
474
475 We have already demonstrated that IgG_1 serum and granuloma levels and serum IgA are
476 undetectable in bolus infected animals at the tissue worm stage (D7), when acute
477 granulomas are present [13]. This contrasts with trickle infected animals, which have
478 acquired partial resistance (Fig 1), have elevated levels of IgG_1^+ PP and MLN plasma cells
479 (Fig 5), and increased levels of serum and granuloma IgG_1 (Fig 3 and 4) during tissue
480 worm development. However, when we passively transferred serum from trickle
481 infected mice to bolus infected animals, we did not detect IgG_1 within their acute
482 granulomas (Sup Fig 4), suggesting that cells, and not only antibodies, present in the
483 granuloma have an important role to play. This supports the idea that sterile immunity
484 may require either extremely high antibody titers, or the activation of additional
485 protective effector cell populations [14].
486
487 IgG-bound macrophages and eosinophils are the cells of the granuloma responsible for
488 parasite damage/death (reviewed in [11]). We found that within the IgG_1^+ cells of the
489 trickle infected animals, $SiglecF^+$ (eosinophils) and $CD206^+$ (macrophages) cells
490 accounted for approximately 50% of the antibody bound cells (Fig 6A, Sup Fig 2 for
491 gating strategy). When comparing the composition of the whole acute granulomas from
492 trickle and bolus infected animals, trickle infected animals had a far higher proportion of
493 $SiglecF^+$ (Fig 6B) and $CD206^+$ cells (Fig 6C) than bolus infected mice. Proportions of $Ly6G^+$

494 (neutrophils, Fig 6C) and NK1.1^{+} (NK cells, Fig 6D) cells remained unchanged between
495 the two groups.
496
497 Resistance in trickle infected mice is therefore associated with the presence of both
498 antibodies and SiglecF^{+}/CD206^{+} cells at the host/parasite interface during tissue
499 development. However, if repeated infections provide protection from Hb, why is this
500 not reflected in nature, where repeated infections are common? Wild rodents have a
501 high incidence of Hb [25,26] and, more generally, intestinal worms are common parasites of
502 humans [1], livestock (reviewed in [2]) and pets [3].
503
504 ***Resistance to Hb in trickle infected animals is lost when they are pre-infected with Tg***
505
506 In natural settings, co-infection is common [28]. This translates to complex host immune
507 environments. To integrate the increased complexity produced by a mixed immune
508 response and potential co-infections into our research, we used *Toxoplasma gondii* (Tg)
509 as a potent inflammatory parasite. The order and time between infections was
510 optimized to ensure minimal pathology while retaining characteristic immune
511 signatures: animals were pre-infected with 10 Tg cysts 14 days prior to trickle Hb
512 infection (Fig 7A). In a previous study using the bolus model of infection, pre-infection
513 with Tg skewed the immune response to a mixed Th1/Th2 Hp immune response by D28.
514 Focusing on the sections with the most granulomas (first half of the small intestine, with
515 SI1 equating to the duodenum and SI2 to the first part of the jejunum), at D21, we found

516 that intestinal levels of *ifnγ* and *il10* gene expression were increased in the jejunum of
517 HbTg trickle infected mice, while *il13* levels were not different (Fig 7B-G). We wanted to
518 determine whether this more complex immune environment would disrupt the effective
519 anti-larval immunity observed during trickle infection, and impact worm burden.
520
521 In this context, we found that pre infection with Tg led to higher worm burdens at both
522 D21 and D28 (Fig 7H). Unsurprisingly, the increased parasite burden was associated with
523 fewer granulomas (Fig 7I) of smaller size (Fig 7J). Taking a closer look at the tissue
524 granulomas from TgHb animals, we found they had decreased levels of IgG_1^+ cells at
525 D21, as observed by flow cytometry (Fig 8A and 8B) and immunofluorescence (Fig 8C).
526 The overall cellular composition of granulomas was also altered: proportions of $SiglecF^+$
527 and $CD206^+$ cells were decreased (Fig 8D and 8E); proportions of $Ly6G^+$ (Fig 8F) and
528 $NK1.1^+$ (Fig 8G) cells remained unchanged. Histology confirmed our flow cytometry
529 findings: HbTg animals had fewer eosinophils (Fig 8H). Interestingly, total macrophages
530 numbers were similar between the two groups (Fig 8I). However, this is likely because
531 similar numbers of macrophages are recruited to the granulomas in both groups.
532 However, in HbTg animals, the influx of CD206+ macrophages is reduced is
533 counterbalanced by the influx of other more inflammatory macrophages.
534
535 To study whether reduced antibody production was responsible for reduced granuloma
536 antibody levels, we measured plasma cell antibody levels at D21 in the MLN using flow
537 cytometry (Fig 9). While total MLN cell numbers were decreased in co-infected animals

538 (Fig 9A), plasma cell percentage and numbers were increased (Fig 9B and 9C). The
539 proportion of MLN IgG_1^+ plasma cells was also increased in TgHb animals (Fig 9D),
540 although their number and antibody production level per cell (MFI) were similar
541 between the two groups (Fig 9E and 9F). However, when focusing on antigen specific
542 IgG_1 producing cells using ELIspot, TgHb animals had far fewer cells than Hb animals: a
543 maximum of 93 vs a mean of 318 (Fig 9G). The difference was not apparent when
544 measuring total IgG_1 (Fig 9H). Finally MLN IgA^+ plasma cells were decreased in number
545 (Fig 9I) but not in proportion (Fig 9J) or in their capacity to make IgA (MFI, Fig 9K).
546 Therefore, in co-infected animals, increased worm burdens are associated with a
547 reduction in the efficacy of granulomas: they lack the presence of $SiglecF^+$ and $CD206^+$
548 cells as well as parasite specific IgG_1.
549
550 **DISCUSSION**
551
552 The pattern of resilience/resistance observed in the laboratory is not what is observed
553 in naturally infected populations of animals – instead, GINs are widespread in wild
554 populations. As an example, studies in wild mice have reported a greater than 60%
555 prevalence with one or more helminth parasites [25–27] and in a recent Albertan survey,
556 100% of cattle herds were found to be infected with intestinal nematodes [40]. This is
557 likely due to stark differences in laboratory conditions compared to natural
558 environments. Factors such as nutrition, age, genetics and environment all play a role.

559 Importantly, so do immune history and co- infection, which can affect the immune
560 system's ability to respond to a parasite infection.
561
562 GIN infections typically occur over extended periods of time, with small amounts of
563 parasite taken up regularly during feeding. The mode of infection is an important factor
564 in the ensuing immune responses. Multiple low dose, or trickle infections, have long
565 been associated with increased resistance to helminth parasites, resulting in a
566 "resistant"/resilient phenotype in animals that are normally considered susceptible [13,41–
567 44]. This acquired resistance can remain long-term, with trickle infected animals
568 maintaining their ability to eliminate worms during subsequent challenge infections [41].
569 Here, we show that effective granulomas are key to eliminating incoming GIN larvae:
570 anti-GIN antibodies must be produced in time to target tissue developing parasites and
571 directed to the host/parasite interface where they can bind activated myeloid cells to
572 immobilise/damage/kill the parasites. Bolus and TgHb trickle infected animals had high
573 worm burdens. In bolus-infected susceptible animals, the antibodies were not produced
574 in time to reach the acute granulomas before the worm exited the tissue. In TgHb
575 trickle-infected animals, granuloma formation was impacted by a reduction in the influx
576 of GIN-specific antibody and myeloid cells to the host-parasite interface.
577
578 Granulomas are formed as a response to tissue invading Hb and consist mainly of
579 macrophages and eosinophils. The exact mechanisms by which tissue developing
580 parasites are immobilised/damaged/destroyed within the granulomas *in vivo* have not

581 been fully characterised. A study involving *Nippostrongylus brasiliensis* (closely related
582 to Hb) infection in mice found that following primary inoculation with the parasite, Th2-
583 primed macrophages remained in the lung (site of parasite development) and facilitated
584 rapid larval clearance upon reinfection [45]. Trickle infection of *N. brasiliensis* in its natural
585 host, the rat, results in increased lung macrophages and eosinophils [46]. We found
586 increased levels of $CD206^+$ cells in the tissue granulomas of trickle infected mice
587 suggesting that long-lived, previously sensitized $CD206^+$ macrophages may also play a
588 direct role in the clearance of Hb tissue stages from the intestine in these animals.
589 During *Litomosoides sigmodontis* infection, a parasite which does not cause granulomas
590 but develops in the pleural cavity, $CD206^+$ pleural cavity macrophage populations
591 increase due to the proliferation of tissue-resident macrophages and, to a lesser extent,
592 the re-programming of recruited inflammatory macrophages [47]. One caveat of our work
593 is that we did not assess markers of tissue residence or recruitment on granuloma
594 macrophages. Without this information, no definite conclusion can be made about the
595 origins of the cells that are required for the effective anti-larval immune response seen
596 in trickle-infected animals.
597
598 *In vitro* and in the presence of immune serum, CD11b on bone marrow derived
599 macrophages can directly bind Hb larvae using complement 3 [16]. This allows FcγR1 to
600 interact with parasite bound $IgG_{2a/c}$ (but not IgG_1) antibodies to immobilize the larvae [15].
601 However, while immune serum allows macrophages to bind to Hp larvae *in vitro*, it does
602 not impact infectivity, suggesting that macrophages are important only in parasite

603 immobilisation and not damage/killing. The authors hypothesised that this rapid
604 activation via $IgG_{2a/c}$ and Fc receptors would likely be important against tissue dwelling
605 parasites during acute infection, but this has yet to be proved as the main mechanism of
606 parasite immobilisation *in vivo*. In accordance with the authors, we observed $CD11b^{+}$
607 antibody-bound macrophages within the worm-containing granulomas of trickle-
608 infected mice. However, only IgG_1, and not $IgG2_c$, was observed in the granulomas
609 which supports previous reports identifying IgG_1 as the protective mechanism in
610 vaccinated mice [48]. Despite their proximity to Hb's infective niche, we saw no increase in
611 IgG_1^{+} plasma cells in the PP of Hb infected animals. This is likely due to parasite-derived
612 immunomodulatory molecules preventing Th2 polarization at this site, as PP in direct
613 contact with Hb larvae show significant expansion of Treg populations [49].
614
615 A recent systematic review has concluded that IgA is associated with partial protection
616 from helminths in mice, rats and sheep [50]. Mechanism of protection include
617 entrapment, neutralization, and eosinophil-mediated ADCC. Mice infected with Hb have
618 elevated IgA levels during primary [17] and repeated [44] infections; mice lacking IgA and
619 infected with Hb in a drug cure/reinfection model do not clear parasites as effectively as
620 wildtype animals [18]. We did not observe IgA within the granulomas of trickle infected
621 animals and did not associate IgA with tissue parasite immobilisation/damage/
622 clearance.
623

624 The role of eosinophils during helminth infection has long been debated (reviewed in
625 [51]). *In vitro* studies have demonstrated that peritoneal and bone marrow derived
626 eosinophils can respectively adhere to [52] and limit the motility of parasitic worm larvae
627 through extracellular traps [53]. Eosinophils obtained from the mammary washes of sheep
628 can kill *Haemonchus contortus* (closely related to Hb) *in vitro* in the presence of
629 antibody; efficacy was increased in the presence of complement and by using 'primed'
630 eosinophils from previously infected sheep [54]. *In vivo,* studies using transgenic animals
631 show that killing by toxic granules is also important: EPX- and MBP1-deficient Balb/c
632 mice have higher worm burdens than wildtype mice after *L. sigmodontis* infection [55].
633 Data from *H. contortus* immunised sheep supports these findings: tissue larvae in the
634 vicinity of eosinophils were found to be at varying stages of damage [56]. However, in Hb
635 infected mice, parasite loads in mice lacking eosinophils (Balb/c Δdbl- GATA-1 and
636 C57Bl/6 PHIL) are similar to wild type animals [57] and others have shown that eosinophils
637 do not adhere to Hb *in vitro* [16], questioning the importance of this cell type in parasite
638 killing. Despite having similar worm burdens, Δdbl- GATA-1 mice challenged with Hb
639 after vaccination had significantly higher numbers of live larvae trapped in their
640 intestinal wall compared to their wild-type counterparts [48]. This suggests that
641 eosinophils are responsible for killing but not immobilising tissue-dwelling parasite
642 stages. The cells likely work in concert with macrophages to limit the number of tissue
643 dwelling parasites that develop into adults, which explains their elevated numbers in the
644 granulomas of trickle infected animals.
645

646 We have previously shown that by 10 days of infection with Tg, a strong increase in IFNγ
647 and IL-10 develops along the whole small intestine, the PP, MLN, SPL and the liver [58].
648 This immune environment impacts the ability of C57Bl/6 mice to mount an effective
649 immune response against a trickle Hb infection. We observed fewer and smaller
650 granulomas; they contained a lesser proportion of $CD206^+$, $SiglecF^+$ and IgG_1-bound
651 cells. To the naked eye, the acute granulomas were not as well formed, and the chronic
652 granulomas did not have the characteristic bead-like appearance that is associated with
653 bolus/trickle infections. Interestingly, in wild mice, granulomas are rarely observed by
654 eye (Pers. Comms. Dr Simon Babayan). This could be due to differences in parasite
655 lifecycles (*H. polygyrus* vs. *H. bakeri*), host responses (wood mice vs. laboratory mice) or
656 could suggest that a more complex immune environment impacts the formation of
657 these structures.
658
659 In a model of allergic inflammation, pre-infection with Tg resulted in decreased serum
660 allergen-specific IgG_1 levels [59]. Despite similar levels of IgG_1-producing plasma cells and
661 IgG_1 production, HbTg infected animals also had reduced antigen specific (Hb) IgG_1^+
662 MLN plasma cell levels compared to Hb trickle infected mice, which helps explain why
663 we observed very little IgG_1^+ in the granulomas of TgHb infected mice. These results
664 reflect gastrointestinal nematode infections in the wild whereby *H. polygyrus* infected
665 mice co-infected with the coccidian *Eimeria* had lower *H. polygyrus*-specific serum IgG_1^+
666 titers than *H. polygyrus* only infected mice [26]. HbTg infected animals also had elevated
667 proportions and numbers of plasma cells, indicating the induction of a polyclonal

668 antibody response against both pathogens, rather than a strong Hb-specific response.
669 The production of polyclonal antibodies during Hb infection has previously been shown
670 to reduce fecundity of adult worms in the intestinal lumen but not to reduce worm
671 burden [18], supporting our findings.
672
673 Despite receiving the same multiple small dose infection as trickle infected animals, the
674 proportion of SiglecF$^+$ and CD206$^+$ cells in the granulomas from co-infected animals was
675 severely reduced, indicating that Tg significantly impaired the recruitment of these cells
676 to the granulomas. TgHb bolus infected mice have been shown to simultaneously
677 decrease proportions of Th2 (GATA3$^+$CD4$^+$) cells and drastically increase proportions of
678 Th1 (T-Bet$^+$CD4$^+$ and T-Bet$^+$CD8$^+$) cells in the small intestine, mesenteric lymph nodes,
679 and spleen [30]. Hb-specific CD4$^+$ T cells produce IFNγ rather than IL-4 or IL-13 *in vitro.* This
680 observed shift would also impact other cells. For example, intestinal epithelial cells
681 recruit eosinophils to the small intestine through the production of eotaxin-1, following
682 activation in a Th2 environment [60]. The impairment of Th2 cytokine production would
683 therefore directly affect the recruitment and activation of eosinophils and CD206$^+$
684 macrophages, both of which are dependent on Th2 cytokine signaling (reviewed in [61,62]).
685 This has also been observed in the context of *N. brasiliensis*. When pre-infected with the
686 apicomplexan *Plasmodium chabaudi* (related to Tg), *N. brasiliensis* co-infected animals
687 had reduced CD206$^+$ macrophage accumulation at the site of parasite development, the
688 lung [63]. When Tg was the pre-infecting parasite, increased shedding of eggs (both in
689 amount of eggs and length of time) was observed in the co-infected animals [64].

690 Increased worm fecundity was also observed in TgHb infected animals using the bolus
691 infection model [30], but unlike with the trickle model, no difference in worm burden was
692 detected.
693
694 Recent work has demonstrated that larval trapping after secondary infection does not
695 require macrophages, rather it is intestinal epithelial cells that play a critical role in this
696 regard [65]. The exact molecules involved remain to be identified, although the process
697 was reliant on IL-4R signalling. The TgHb mice had significantly increased levels of
698 intestinal *ifnγ* levels throughout the experiment which may have hampered the IEC IL-4R
699 signalling required for effective clearance.
700
701 NK and neutrophils proportions did not change with the mode of infection. Recent work
702 has argued that NK cells are essential for host protection during the acute phase of Hb
703 infection. Removing NK cells did not impact worm burden or fitness in the bolus mode
704 of infection, rather intestinal injury was increased [66]. Ly6G^{+} cells have been identified
705 within the granulomas of Hb infected animals [67,68]. However, immunity to Hb following
706 vaccination was unaffected by the loss of neutrophils induced by antibody treatment in
707 C57Bl/6 animals [48], and neutrophil populations did not increase in the lungs of mice with
708 a secondary *N. brasiliensis* infection [45].
709
710 One limitation of our study is that we did not assess whether differences in the
711 microbiome could account for the changes we observed. In the laboratory setting, Tg

712 infection (Me49, oral gavage) leads to dysbiosis, characterised by an increase in
713 proinflammatory Pseudomonadota species and a reduction of beneficial commensal
714 species, that persists into the chronic stage of infection [69]. By contrast, Hb infection in
715 C57Bl/6 mice leads to duodenal increases in the abundance of the immunoregulatory
716 *Lactobacillus* species [70] and infections in germ free mice result in increased worm
717 burdens [71]. However, in experiments using the trickle, rather than bolus, infection
718 model it was demonstrated that mice infected with *Trichuris muris* recovered alpha
719 diversity following the development of resistance [41]. Interestingly, in mice infected with
720 *T. muris* which were then moved outdoors and acquired an enriched microbiome, the
721 authors measured a decrease in Th2 and increase in Th1 immunity associated with
722 increased worm burdens and biomass [72], somewhat reflecting the more nuanced
723 immune environments created in our co-infection model. However, it is also important
724 to remember that other factors, unrelated to host biology, such as temperature and
725 humidity which are strong moderators of the microbiome [73], may play a significant role
726 in infection outcome in the wild. And that restricting studies to Th1 vs. Th2 in a
727 particular setting at a particular timepoint likely oversimplifies the mechanisms
728 underlying the optimal host response [74]. However, compared to both the typical
729 experimental infection (bolus) and the single infection grazing type infection (trickle),
730 the co-infection trickle model described here more realistically reflects immune
731 responses in real-world infections. Feeding through grazing exposes hosts to a variety of
732 pathogens. While our two-parasite system is not nearly as complex as real-world

infections, our research begins to explain the overwhelming prevalence of helminth infections worldwide.

ACKNOWLEDGEMENTS

This works was funded through Dr Finney's grants from the Canadian Foundation for Innovation and the Natural Sciences and Engineering Research Council of Canada (NSERC), as well as scholarships for Drs Anupama Ariyaratne (NSERC Create in Host Parasite Interactions), Shashini Perera (Alberta Graduate Excellence Scholarship), Naomi Chege (Graeme Bell and Norma Kay Sullivan-Bell Graduate Scholarship in Biology), Emma Forrester (University of Calgary PURE Scholarship), Mayara Luzzi (Mitacs Globalink), Joel Bowron (NSERC), Edina Szabo (UCalgary Eyes High). The funders had no role in study design, analysis or reporting.

COMPETING INTERESTS STATEMENT

The authors declare that they have no known competing financial interests or personal relationships that could have appeared to influence the work reported in this paper.

DATA ACCESS

All data not available in the manuscript or supplemental materials are available from the corresponding author upon request.

REFERENCES

1. Montresor, A. *et al.* The global progress of soil-transmitted helminthiases control in 2020 and World Health Organization targets for 2030. *PLOS Neglected Tropical Diseases* **14**, e0008505 (2020).
2. Vercruysse, J. *et al.* Control of helminth ruminant infections by 2030. *Parasitology* **145**, 1655–1664 (2018).
3. Mohamed, A. S., Moore, G. E. & Glickman, L. T. Prevalence of intestinal nematode parasitism among pet dogs in the United States (2003-2006). *J Am Vet Med Assoc* **234**, 631–637 (2009).
4. Brooker, S. Estimating the global distribution and disease burden of intestinal nematode infections: Adding up the numbers – A review. *International Journal for Parasitology* **40**, 1137–1144 (2010).
5. Mavrot, F., Hertzberg, H. & Torgerson, P. Effect of gastro-intestinal nematode infection on sheep performance: a systematic review and meta-analysis. *Parasites Vectors* **8**, 557 (2015).
6. Claerebout, E. & Vercruysse, J. The immune response and the evaluation of acquired immunity against gastrointestinal nematodes in cattle: a review. *Parasitology* **120**, 25–42 (2000).

7. Stevens, L. *et al.* Ancient diversity in host-parasite interaction genes in a model parasitic nematode. *Nat Commun* **14**, 7776 (2023).
8. Reynolds, L. a., Filbey, K. J. & Maizels, R. M. Immunity to the model intestinal helminth parasite Heligmosomoides polygyrus. *Seminars in Immunopathology* **34**, 829–846 (2012).
9. Urban, J. F. J., Katona, I. M., Paul, W. E. & Finkelman, F. D. Interleukin 4 is important in protective immunity to a gastrointestinal nematode infection in mice. *Proceedings of the National Academy of Sciences of the United States of America* **88**, 5513–5517 (1991).
10. Allison Bancroft, G. J., J McKenzie, A. N., Bancroft, A. J. & Grencis, R. K. Intestinal Nematode Infection A Critical Role for IL-13 in Resistance to A Critical Role for IL-13 in Resistance to Intestinal Nematode Infection 1. *J Immunol References* **160**, 3453–3461 (1998).
11. Ariyaratne, A. & Finney, C. A. M. Eosinophils and macrophages within the Th2-induced granuloma: Balancing killing and healing in a tight space. *Infection and Immunity* **87**, e00127-19 (2019).
12. Filbey, K. J. *et al.* Innate and adaptive type 2 immune cell responses in genetically controlled resistance to intestinal helminth infection. *Immunology and cell biology* **92**, 436–48 (2014).
13. Ariyaratne, A. *et al.* Trickle infection with Heligmosomoides polygyrus results in decreased worm burdens but increased intestinal inflammation and scarring. *Front. Immunol.* **13**, 1020056 (2022).

14. Hewitson, J. P. *et al.* Concerted Activity of IgG1 Antibodies and IL-4/IL-25-Dependent Effector Cells Trap Helminth Larvae in the Tissues following Vaccination with Defined Secreted Antigens, Providing Sterile Immunity to Challenge Infection. *PLOS Pathogens* **11**, e1004676 (2015).
15. Esser-von Bieren, J. *et al.* Antibody-Mediated Trapping of Helminth Larvae Requires CD11b and Fcγ Receptor I. *J Immunol* **194**, 1154–1163 (2015).
16. Esser-von Bieren, J. *et al.* Antibodies trap tissue migrating helminth larvae and prevent tissue damage by driving IL-4R-independent alternative differentiation of macrophages. *PLoS Pathogens* **9**, e1003771 (2013).
17. Ben-Smith, Wahid, Lammas, & Behnke The relationship between circulating and intestinal Heligmosomoides polygyrus-specific IgG1 and IgA and resistance to primary infection. *Parasite Immunology* **21**, 383–395 (1999).
18. McCoy, K. D. *et al.* Polyclonal and specific antibodies mediate protective immunity against enteric helminth infection. *Cell Host Microbe* **4**, 362–373 (2008).
19. Wahid, F. N. & Behnke, J. M. Immunological relationships during primary infection with Heligmosomoides polygyrus (Nematospiroides dubius): parasite specific IgG1 antibody responses and primary response phenotype. *Parasite immunology* **15**, 401–413 (1993).
20. Wahid, F. N., Behnke, J. M., Grencis, R. K., Else, K. J. & Ben-Smith, A. W. Immunological relationships during primary infection with Heligmosomoides polygyrus: Th2 cytokines and primary response phenotype. *Parasitology* **108 (Pt 4**, 461–471 (1994).

21. Dobson, C. Passive transfer of immunity with serum in mice infected with Nematospiroides dubius: influence of quality and quantity of immune serum. *International journal for parasitology* **12**, 207–213 (1982).

22. Pritchard, D. I., Williams, D. J., Behnke, J. M. & Lee, T. D. The role of IgG1 hypergammaglobulinaemia in immunity to the gastrointestinal nematode Nematospiroides dubius. The immunochemical purification, antigen-specificity and in vivo anti-parasite effect of IgG1 from immune serum. *Immunology* **49**, 353–365 (1983).

23. Pritchard, D. I., Behnke, J. M. & Williams, D. J. Primary infection sera and IgG1 do not block host-protective immunity to Nematospiroides dubius. *Immunology* **51**, 73–81 (1984).

24. Williams, D. J. & Behnke, J. M. Host protective antibodies and serum immunoglobulin isotypes in mice chronically infected or repeatedly immunized with the nematode parasite Nematospiroides dubius. *Immunology* **48**, 37–47 (1983).

25. Babayan, S. A., Liu, W., Hamilton, G. & Kilbride, E. The immune and non-immune Pathways That Drive chronic gastrointestinal helminth Burdens in the Wild. *Frontiers in Immunology* **9**, 1–12 (2018).

26. Clerc, M., Devevey, G., Fenton, A. & Pedersen, A. B. Antibodies and coinfection drive variation in nematode burdens in wild mice. *International Journal for Parasitology* **48**, 785–792 (2018).

27. Lewis, J. W., Morley, N. J. & Behnke, J. M. Helminth parasites of the wood mouse Apodemus sylvaticus in Southern England: levels of infection, species richness and interactions between species. *Journal of Helminthology* **97**, e18 (2023).

28. Hoarau, A. O. G., Mavingui, P. & Lebarbenchon, C. Coinfections in wildlife: Focus on a neglected aspect of infectious disease epidemiology. *PLOS Pathogens* **16**, e1008790- (2020).
29. Snyder, L. M. & Denkers, E. Y. From Initiators to Effectors: Roadmap Through the Intestine During Encounter of Toxoplasma gondii With the Mucosal Immune System. *Front Cell Infect Microbiol* **10**, 614701 (2021).
30. Ahmed, N. *et al.* Toxoplasma Co-infection Prevents Th2 Differentiation and Leads to a Helminth-Specific Th1 Response. *Frontiers in Cellular and Infection Microbiology* **7**, 1–12 (2017).
31. Ariyaratne, A., Szabo, E. K., Bowron, J. & Finney, C. A. M. Increases in helminth-induced IL-21 protein levels disappear upon sample freezing. *Cytokine* **108**, 179–181 (2018).
32. Pfaffl, M. W. Relative quantification. 63–82 (2004).
33. McKenzie, G. J., Fallon, P. G., Emson, C. L., Grencis, R. K. & McKenzie, A. N. Simultaneous disruption of interleukin (IL)-4 and IL-13 defines individual roles in T helper cell type 2-mediated responses. *J Exp Med* **189**, 1565–1572 (1999).
34. Urban, J. F. *et al.* IL-13, IL-4Ralpha, and Stat6 are required for the expulsion of the gastrointestinal nematode parasite Nippostrongylus brasiliensis. *Immunity* **8**, 255–264 (1998).
35. Oeser, K., Schwartz, C. & Voehringer, D. Conditional IL-4/IL-13-deficient mice reveal a critical role of innate immune cells for protective immunity against gastrointestinal helminths. *Mucosal Immunol* **8**, 672–682 (2015).

36. Pernthaner, A. *et al.* Cytokine and antibody subclass responses in the intestinal lymph of sheep during repeated experimental infections with the nematode parasite *Trichostrongylus colubriformis*. *Veterinary Immunology and Immunopathology* **114**, 135–148 (2006).
37. Hasnain, S. Z. *et al.* Muc5ac: a critical component mediating the rejection of enteric nematodes. *J Exp Med* **208**, 893–900 (2011).
38. Shea-Donohue, T. *et al.* Role of enteric nerves in immune-mediated changes in protease-activated receptor 2 effects on gut function. *Neurogastroenterol Motil* **22**, 1138-e291 (2010).
39. King, I. L., Mohrs, K. & Mohrs, M. A nonredundant role for IL-21 receptor signaling in plasma cell differentiation and protective type 2 immunity against gastrointestinal helminth infection. *J Immunol* **185**, 6138–6145 (2010).
40. Avramenko, R. W. *et al.* The use of nemabiome metabarcoding to explore gastro-intestinal nematode species diversity and anthelmintic treatment effectiveness in beef calves. *International Journal for Parasitology* **47**, 893–902 (2017).
41. Glover, M., Colombo, S. A. P., Thornton, D. J. & Grencis, R. K. Trickle infection and immunity to Trichuris muris. *PLoS Pathogens* **15**, e1007926 (2019).
42. Colombo, S. Polyparasitism of Gastrointestinal Helminths. (2019).at <https://www.research.manchester.ac.uk/portal/files/160457498/FULL_TEXT.PDF>
43. Brailsford, T. J. & Behnke, J. M. The dynamics of trickle infections with Heligmosomoides polygyrus in syngeneic strains of mice. *International Journal for Parasitology* **22**, 351–359 (1992).

44. Behnke, J. M., Lowe, A., Clifford, S. & Wakelin, D. Cellular and serological responses in resistant and susceptible mice exposed to repeated infection with Heligmosomoides polygyrus bakeri. *Parasite Immunology* **25**, 333–340 (2003).

45. Chen, F. *et al.* Neutrophils prime a long-lived effector macrophage phenotype that mediates accelerated helminth expulsion. *Nature Immunology 2014 15:10* **15**, 938–946 (2014).

46. Ferens, W. A., Arai, H. P. & Befus, A. D. Bronchoalveolar Leucocyte Responses to Trickle Infections with Nippostrongylus brasiliensis in Rats. *The Journal of Parasitology* **80**, 654–656 (1994).

47. Jenkins, S. J. *et al.* Local macrophage proliferation, rather than recruitment from the blood, is a signature of Th2 inflammation. *Science* **332**, 1284–1288 (2011).

48. Hewitson, J. P. *et al.* Concerted activity of IgG1 antibodies and IL-4/IL-25-dependent effector cells trap helminth larvae in the tissues following vaccination with defined secreted antigens, providing sterile immunity to challenge infection. *PLoS Pathogens* **11**, 1–22 (2015).

49. Mosconi, I. *et al.* Parasite proximity drives the expansion of regulatory T cells in Peyer's patches following intestinal helminth infection. *Infection and Immunity* **83**, 3657–3665 (2015).

50. Ramos, A. C. S. *et al.* The role of IgA in gastrointestinal helminthiasis: A systematic review. *Immunology Letters* **249**, 12–22 (2022).

51. Mitre, E. & Klion, A. D. Eosinophils and helminth infection: protective or pathogenic? *Semin Immunopathol* **43**, 363–381 (2021).

52. Pincus, S. H. & Cammarata, P. Eosinophil adherence to infective larvae of Trichinella spiralis: quantification and modulation. *Immunology* **56**, 219–225 (1985).
53. Ehrens, A. *et al.* Eosinophils and Neutrophils Eliminate Migrating Strongyloides ratti Larvae at the Site of Infection in the Context of Extracellular DNA Trap Formation. *Front Immunol* **12**, 715766 (2021).
54. Rainbird, M. A., Macmillan, D. . & Meeusen, E. N. T. . Eosinophil-mediated killing of Haemonchus contortus larvar: effect of eosinophil activation and role of antobody, complement and interleukin-5. *Parasite Immunology* **20**, 93–103 (1998).
55. Specht, S. *et al.* Lack of eosinophil peroxidase or major basic protein impairs defense against murine filarial infection. *Infection and Immunity* **74**, 5236–5243 (2006).
56. Balic, A., Cunningham, C. P. & Meeusen, E. N. T. Eosinophil interactions with Haemonchus contortus larvae in the ovine gastrointestinal tract. *Parasite Immunology* **28**, 107–115 (2006).
57. Strandmark, J. *et al.* Eosinophils are required to suppress Th2 responses in Peyer's patches during intestinal infection by nematodes. *Mucosal Immunol* **10**, 661–672 (2017).
58. Szabo, E. K. *et al.* Heligmosomoides bakeri and Toxoplasma gondii co-infection leads to increased mortality associated with intestinal pathology. 2021.05.27.445631 (2023).doi:10.1101/2021.05.27.445631
59. Wagner, A. *et al.* Immunoregulation by *Toxoplasma gondii* infection prevents allergic immune responses in mice. *International Journal for Parasitology* **39**, 465–472 (2009).

60. Kim, E. *et al.* Intestinal Epithelial Cells Regulate Gut Eotaxin Responses and Severity of Allergy. *Front. Immunol*. **9**, (2018).
61. Gordon, S. & Martinez, F. O. Alternative activation of macrophages: mechanism and functions. *Immunity* **32**, 593–604 (2010).
62. Shah, K., Ignacio, A., McCoy, K. D. & Harris, N. L. The emerging roles of eosinophils in mucosal homeostasis. *Mucosal Immunol* **13**, 574–583 (2020).
63. Hoeve, M. A. *et al*. Plasmodium chabaudi limits early Nippostrongylus brasiliensis-induced pulmonary immune activation and Th2 polarization in co-infected mice. *BMC Immunol* **10**, 60 (2009).
64. Liesenfeld, O., Dunay, I. R. & Erb, K. J. Infection with Toxoplasma gondii Reduces Established and Developing Th2 Responses Induced by Nippostrongylus brasiliensis Infection. *Infection and Immunity* **72**, 3812–3822 (2004).
65. Westermann, S. *et al*. Th2-dependent STAT6-regulated genes in intestinal epithelial cells mediate larval trapping during secondary Heligmosomoides polygyrus bakeri infection. *PLOS Pathogens* **19**, e1011296 (2023).
66. Gentile, M. E. *et al.* NK cell recruitment limits tissue damage during an enteric helminth infection. *Mucosal Immunol* **13**, 357–370 (2020).
67. Anthony, R. M. *et al.* Memory T(H)2 cells induce alternatively activated macrophages to mediate protection against nematode parasites. *Nature medicine* **12**, 955–60 (2006).
68. Morimoto, M. *et al.* Peripheral CD4 T cells rapidly accumulate at the host:parasite interface during an inflammatory Th2 memory response. *Journal of immunology* **172**, 2424–2430 (2004).

69. French, T. *et al.* Persisting Microbiota and Neuronal Imbalance Following T. gondii Infection Reliant on the Infection Route. *Front. Immunol.* **13**, (2022).
70. Reynolds, L. A. *et al.* Commensal-pathogen interactions in the intestinal tract: Lactobacilli promote infection with, and are promoted by, helminth parasites. *Gut Microbes* **5**, 522–532 (2014).
71. Moyat, M. *et al.* Microbial regulation of intestinal motility provides resistance against helminth infection. *Mucosal Immunol* **15**, 1283–1295 (2022).
72. Leung, J. M. *et al.* Rapid environmental effects on gut nematode susceptibility in rewilded mice. *PLOS Biology* **16**, e2004108 (2018).
73. Bär, J. *et al.* Strong effects of lab-to-field environmental transitions on the bacterial intestinal microbiota of Mus musculus are modulated by Trichuris murisinfection. *FEMS Microbiology Ecology* **96**, fiaa167 (2020).
74. Liu, W. *et al.* Vaccine-induced time- and age-dependent mucosal immunity to gastrointestinal parasite infection. *npj Vaccines* **7**, 1–9 (2022).

FIGURE LEGENDS

Figure 1: Characteristics of the H. bakeri trickle infection model in C57Bl/6 mice. C57Bl/6 mice were infected with 200 *H. bakeri* according to the bolus and trickle infection regimes. (A) Trickle infection regime: mice are infected with 200 larvae in total, but in multiple doses over the course of infection (in blue). Doses of 20 larvae are trickled on days 0, 2, 4, 6, 8, 10, 12, 14, 16 and 18 post-infection This leaves a 10-day window after the final dose to allow parasites to fully develop into adults and migrate

977 from the intestinal tissue to the intestinal lumen. Bolus infected mice were infected with
978 200 larvae at day 0 (in red). Adult worms (B) and granulomas (C) were counted in the
979 small intestine at D28. Mice were infected according to the bolus (red) and trickle (blue)
980 regimes. Total granuloma area (D) and the granuloma necrotic centre (E) were
981 measured on H and E stained slides of whole small intestine. Macrophages (F) and
982 eosinophil (G) were counted within the center of the granulomas at x400 magnification.
983 Cells were counted for one field of view (FOV) per granuloma. Graphs represent pooled
984 data from a minimum of 2 experiments, bars represent the median, with a minimum of
985 3 mice per group per experiment. A normality test (D'Agostino & Pearson) was
986 performed, followed by a Kruskal Wallis/Anova (with post-tests) and Mann Whitney/T-
987 test to test for statistical significance between trickle and bolus groups, n.s. = not
988 significant, *** = $p<0.001$, **** = $p<0.001$.
989
990 ***Figure 2: Th2 response in the SPL, MLN, PP and SI during H. bakeri trickle infection in***
991 ***C57Bl/6 mice.*** C57Bl/6 mice were infected with 200 *H. bakeri* larvae according to the
992 bolus and trickle infection regimes. At D28, single cell suspensions were isolated from
993 the spleen (SPL) ,mesenteric lymph nodes (MLN) and Peyers Patches (PP) and cultured
994 for 48 hours in the presence of Hb antigen. (A-D) IL-4 and IL-13 MLN and SPL cytokine
995 levels were measured in the supernatant by ELISA. Total cell numbers were calculated
996 for the MLN (E) and SPL (F). IL-4 (G) and IL-13 (H) PP cytokine levels were measured in
997 the supernatant by ELISA. (I-M) Small intestines were dissected and scraped using a
998 glass slide leaving only the serosa. (I-J) IL-4, and IL-13, were measured in the intestinal

999 scrapings by ELISA. (K) The intestinal scrapings were weighed for each mouse and
1000 normalised to control animals. (L) Mice were fasted for 6 hours followed by Evans Blue
1001 administration. Time from dye administration to the passing of dyed fecal pellets was
1002 measured and normalised to control animals. (M) IL-21 was measured in the intestinal
1003 scrapings by ELISA. Mice were infected according to the bolus (red) and trickle (blue)
1004 regimes. Naive mice are represented by grey circles. Graphs represent pooled data from
1005 2 experiments, bars represent the median, with a minimum of 3 mice per group per
1006 experiment. A normality test (D'Agostino & Pearson) was performed, followed by a
1007 Kruskal Wallis/Anova (with post-tests) for statistical significance between trickle and
1008 bolus groups, n.s. = not significant, * = $p<0.05$, ** = $p<0.01$, *** = $p<0.001$, **** =
1009 $p<0.001$.
1010
1011 ***Figure 3: Antibody levels during H. bakeri trickle infection in C57Bl/6 mice.*** C57Bl/6
1012 mice were infected with 200 *H. bakeri* larvae according to the bolus and trickle infection
1013 regimes. At D28, blood was collected and serum obtained. (A) Total serum IgE, (B) Total
1014 serum IgG_1, (C) Parasite-specific serum IgG_1 and (D) Total intestinal IgA were measured
1015 by ELISA. Levels in naïve controls were undetectable for parasite specific IgG_1. Graphs
1016 represent pooled data from a minimum of 2 experiments, bars represent the median,
1017 with a minimum of 3 mice per group per experiment. A normality test (D'Agostino &
1018 Pearson) was performed, followed by a Kruskal Wallis/Anova (with post-tests) and
1019 Mann Whitney/T-test to test for statistical significance between trickle and bolus
1020 groups, n.s. = not significant, ** = $p<0.01$, *** = $p<0.001$.

1021

1022 ***Figure 4: IgG$_1$ in the granulomas of trickle-H. bakeri infected C57Bl/6 mice.*** C57Bl/6

1023 mice were infected with 200 *H. bakeri* according to bolus and/or trickle models of

1024 infection. (A) Trickle infection regimen (worm-containing granulomas): mice are infected

1025 with 200 larvae in total but spread out over infection (in blue). Mice are euthanised on

1026 day 21, doses of 20 larvae are trickled on days 0, 2, 4, 6, 8, 10, 12, 14, 16 and 18 post-

1027 infection. There is a 3 day window after the final dose to allow parasites to start

1028 developing in the mucosa and observe the formation of granulomas around them, as

1029 well as having mature worms in the lumen. For the comparative bolus infections, we are

1030 using animals infected for 5 (tissue worms only) and 21 (worms found in the lumen only)

1031 days. (B & H) Granulomas were isolated from the small intestine of 5 mice per group.

1032 Granulomas from the individual animals were pooled to form one sample per group.

1033 Cells were obtained by tissue digestion of the pooled samples and stained by flow

1034 cytometry. (B) The percentage of CD11b$^+$IgG$_1^+$ cells as a proportion of live granuloma

1035 cells (with T and B cells removed) from acute granulomas was calculated for three

1036 independent experiments. (C) Representative flow cytometry plots showing IgG$_1$ and

1037 CD11b expression on live granuloma cells from acute granulomas. (D-G) Formalin fixed,

1038 paraffin-embedded sections were obtained from small intestine swiss rolls. These

1039 sections were co-stained with DAPI and either anti-mouse (D) IgG$_1$, (E) IgG$_{2c}$, (F) IgA/IgE

1040 and (G) IgG$_1$. Scale bar=100µm. Antibody stain (left), isotype control stain (right).

1041 Representative granulomas (white lines) containing worms (acute granulomas, D-F) or

1042 not containing worms (chronic granulomas, G) from trickle and bolus infected mice. (H)

1043 The percentage of $CD11b^{+}IgG_1^{+}$ cells as a proportion of live granuloma cells (with T and B
1044 cells removed) from chronic granulomas was calculated for three independent
1045 experiments. (I) Representative flow cytometry plots showing IgG_1 and CD11b
1046 expression on live granuloma cells from chronic granulomas. (J) Total granuloma area
1047 (K) and the granuloma necrotic centre were measured for chronic granulomas on H and
1048 E stained formalin fixed sections from whole small intestine swiss rolls. Graphs
1049 represent pooled data from a minimum of 2 experiments, bars represent the median,
1050 with a minimum of 3 mice per group per experiment. A normality test (D'Agostino &
1051 Pearson) was performed, followed by Mann Whitney/T-test to test for statistical
1052 significance between trickle and bolus groups, n.s. = not significant, * = $p<0.05$, ** =
1053 $p<0.01$.
1054
1055 ***Figure 5: MLN and PP plasma cell antibody production during H. bakeri infection in***
1056 ***C57Bl/6 mice.*** C57Bl/6 mice were infected with 200 *H. bakeri* larvae according to the
1057 bolus and trickle infection regimes. Mice were euthanized at D21. Mesenteric lymph
1058 node (MLN) and Peyer's Patches (PP) were isolated to obtain single cell suspensions
1059 which were analysed by flow cytometry. (A) The proportion of MLN $CD138^{+}$ (plasma)
1060 cells. (B) Representative histogram showing CD138 expression. (C) The proportion of PP
1061 $CD138^{+}$ cells. (D) The number of MLN $CD138^{+}$ cells. The proportion of MLN (E) and PP (F)
1062 $CD138^{+}$ cells expressing intracellular IgG_1. (G) The number of MLN $CD138^{+}$ cells
1063 expressing intracellular IgG1. (H) Representative flow plots showing IgA and IgG
1064 expression on MLN $CD138^{+}$ cells. The proportion of MLN (I) and PP (J) $CD138^{+}$ cells

1065 expressing intracellular IgA. (K) The number of MLN $CD138^+$ cells expressing intracellular
1066 IgA. The IgG_1 MFI of MLN (L) and PP (M) $CD138^+$ cells expressing intracellular IgG1. The
1067 IgG_1 MFI of MLN (N) and PP (O) $CD138^+$ cells expressing intracellular IgG1. Graphs
1068 represent pooled data from a minimum of 3 experiments, bars represent the median,
1069 with a minimum of 5 mice per group per experiment. A normality test (D'Agostino &
1070 Pearson) was performed, followed by a Kruskal Wallis/Anova (with post tests) and Mann
1071 Whitney/T-test to test for statistical significance between trickle and bolus groups, n.s. =
1072 not significant, * = $p<0.05$, ** = $p<0.01$, *** = $p<0.001$, **** = $p<0.001$.
1073
1074 ***Figure 6: Acute granuloma cell composition.*** C57Bl/6 mice were infected with 200 *H.*
1075 *bakeri* according to bolus and/or trickle models of infection and euthanised at D21.
1076 Granulomas were isolated from the small intestine of 5 mice per group. Granulomas
1077 from the individual animals were pooled to form one sample per group. Cells were
1078 obtained by tissue digestion of the pooled samples and surface stained by flow
1079 cytometry. (A) Proportions of IgG_1-bound cells ($SiglecF^+$, $CD206^+$, $Ly6G^+$ and $NK1.1^+$)
1080 were calculated within the acute (worm containing) granulomas of trickle infected mice.
1081 Numbers reflect the mean of five independent experiments. Proportions of acute
1082 granuloma (B) $SiglecF^+$, (C) $CD206^+$, (D) $Ly6G^+$ and (E) $NK1.1^+$ cells within bolus and trickle
1083 infected mice were calculated for three independent experiments. A paired T-test to
1084 test for statistical significance between trickle and bolus groups was performed, n.s. =
1085 not significant, * = $p<0.05$, *** = $p<0.001$.
1086

1087 ***Figure 7: The T. gondii/H. bakeri trickle coinfection model in C57Bl/6 mice.*** C57Bl/6
1088 mice were infected with 200 *H. polygyrus* according to the coinfection and trickle
1089 infection regimes. (A) Coinfection trickle infection regime: mice are infected with 20
1090 Me49 *T. gondii* cysts 14 days prior to *H. bakeri* infection which consists of 200 larvae in
1091 total, but in multiple doses over the course of infection (in grey). Doses of 20 larvae are
1092 trickled on days 0, 2, 4, 6, 8, 10, 12, 14, 16 and 18 post-infection Animals are euthanised
1093 on D21 (3 day window after the final dose), where tissue and lumen parasites can be
1094 observed. Animals are also euthanised on D28 (10-day window after the final dose),
1095 where only lumen parasites are found. Mice were infected according to the Hb (blue)
1096 and TgHb (purple) regimes. (B-G) RNA was extracted was from the small intestine, which
1097 had been cut into four equal portions. The duodenum (SI1) and jejunum (SI2) were
1098 used. Gene expression was measured by quantitative RT-PCR for *il13* (B & C), *ifnγ*(D & E)
1099 and *Il10* (F & G). Adult worms (H) and granulomas (I) were counted in the small intestine
1100 at D21 and D28. (J) Granuloma area in C57Bl/6 mice was measured on H and E stained
1101 sections from whole small intestine swiss rolls. Graphs represent pooled data from a
1102 minimum of 2 experiments, bars represent the median, with a minimum of 4 mice per
1103 group per experiment. A normality test was performed, followed by a Kruskal
1104 Wallis/Anova (with post-tests) and Mann Whitney to test for statistical significance
1105 between Hb and HbTg groups, n.s. = not significant, ** = $p<0.01$, ***= $p<0.001$, **** =
1106 $p<0.0001$.
1107

1108 ***Figure 8: Granuloma characteristics in the T. gondii/H. bakeri trickle coinfection model***
1109 ***in C57Bl/6 mice.*** C57Bl/6 mice were infected with 200 *H. bakeri* according to the trickle
1110 single or co-infection models, and euthanised on D21. Co-infected animals are infected
1111 with 10 cysts of Me49 *T. gondii* 14 days before the first *H. bakeri* dose. Granulomas
1112 were isolated from the small intestine of 5 mice per group. Granulomas from the
1113 individual animals were pooled to form one sample per group. Cells were obtained by
1114 tissue digestion of the pooled samples and stained by flow cytometry. (A) The
1115 percentage of $CD11b^{+}IgG_1^{+}$ cells as a proportion of live granuloma cells (with T and B
1116 cells removed) from acute granulomas was calculated for three independent
1117 experiments. (B) Representative flow cytometry plots showing IgG_1 and CD11b
1118 expression on live granuloma cells from acute granulomas. (C) Formalin fixed, paraffin-
1119 embedded sections were obtained from small intestine swiss rolls. These sections were
1120 co-stained with DAPI and anti-mouse IgG_1. Scale bar=100µm. Antibody stain (left),
1121 isotype control stain (right). Representative granulomas (white lines) containing worms
1122 (acute granulomas) from trickle and co-infected mice. (D) Proportions of acute
1123 granuloma (D) $SiglecF^{+}$, (E) $CD206^{+}$, (F) $Ly6G^{+}$ and (G) $NK1.1^{+}$ cells within trickle and co-
1124 infected mice were calculated for three independent experiments. A paired T-test to
1125 test for statistical significance between two groups was performed, n.s. = not significant,
1126 * = $p<0.05$. Granulomas were identified on H and E stained slides of whole small
1127 intestine. Eosinophils (H) and macrophages (I) were counted within the center of the
1128 granulomas at x400 magnification. Cells were counted for one field of view (FOV) per
1129 granuloma. A normality test was performed, followed by a Kruskal Wallis/Anova (with

1130 post-tests) to test for statistical significance between trickle and co-infected groups, n.s.
1131 = not significant, * = $p<0.05$, **** = $p<0.001$.
1132
1133 ***Figure 9: Plasma cell and antibody dynamics in T. gondii/H. bakeri trickle co-infected***
1134 ***C57Bl/6 mice.*** C57Bl/6 mice were infected with 200 *H. bakeri* according to the trickle
1135 single or co-infection models, and euthanised on D21. Co-infected animals are infected
1136 with 10 cysts of Me49 *T. gondii* 14 days before the first *H. bakeri* dose. Mesenteric
1137 lymph nodes (MLN) were isolated to obtain single cell suspensions which were analysed
1138 by flow cytometry. (A) The number of total viable MLN cells. (B) The proportion of
1139 $CD138^+$ (plasma) cells. (C) The number of $CD138^+$ cells. (D) The proportion of $CD138^+$
1140 cells expressing intracellular IgG_1. (E) The number of $CD138^+$ cells expressing
1141 intracellular IgG_1. (F) The IgG_1 MFI of $CD138^+$ cells expressing intracellular IgG_1. The
1142 number of MLN *H. bakeri*-specific (G) and total (H) IgG_1 producing cells assessed by
1143 ELISPOT. (I) The proportion of $CD138^+$ cells expressing intracellular IgA. (J) The number
1144 of $CD138^+$ cells expressing intracellular IgA. (K) The IgA MFI of $CD138^+$ cells expressing
1145 intracellular IgG_1. Graphs represent pooled data from a minimum of 2 experiments, bars
1146 represent the median, with a minimum of 5 mice per group per experiment. A normality
1147 test (D'Agostino & Pearson) was performed, followed by a Kruskal Wallis/Anova (with
1148 post-tests) and Mann Whitney/T-test to test for statistical significance between Hb and
1149 TgHb groups, n.s. = not significant, * = $p<0.05$, ** = $p<0.01$, **** = $p<0.001$.
1150

1151 ***Supplemental Figure 1: Characteristics of the H. bakeri trickle infection model in Balb/c***
1152 ***mice.*** Balb/c mice were infected with 200 *H. bakeri* according to the bolus and trickle
1153 infection regimes. Adult worms (A) and granulomas (B) were counted in the small
1154 intestine at D28. Mice were infected according to the bolus (red) and trickle (blue)
1155 regimes. Single cell suspensions were isolated from the spleen (SPL) and mesenteric
1156 lymph nodes (MLN) and cultured for 48 hours in the presence of Hb antigen. MLN/SPL
1157 cell numbers were calculated (C & F), and IL-4 (D & G) and IL-13 (E & H) cytokine levels
1158 were measured in the supernatant by ELISA. (I) Total serum IgE, (J) total serum IgG_1 and
1159 (K) parasite-specific serum IgG_1 were measured by ELISA. Levels in naïve controls were
1160 undetectable for parasite specific IgG_1. A normality test (D'Agostino & Pearson) was
1161 performed, followed by a Kruskal Wallis/Anova (with post-tests) and Mann Whitney/T-
1162 test to test for statistical significance between trickle and bolus groups, n.s. = not
1163 significant, ** = $p<0.01$, *** = $p<0.001$, **** = $p<0.001$.
1164
1165 ***Supplementary Figure 2: Gating strategy for IgG_1^+ granuloma cells.*** Granulomas (acute
1166 and chronic) were isolated from the small intestine of 5 mice per group. Granulomas
1167 from the individual animals were pooled to form one sample per group. Cells were
1168 obtained by tissue digestion of the pooled samples and surface stained by flow
1169 cytometry. Gating strategy involved removing doublets using FSC and SSC. Dead cells
1170 (positive for viability stain) were excluded. B and T cells were excluded by removing
1171 $CD3^+$ and $CD19^+$ cells from the analysis. Antibody-bound cells were identified as
1172 $CD11b^+IgG_1^+$ cells using appropriate controls. To identify specific cell types, eosinophils

1173 were identified as SiglecF$^+$, macrophages as CD206$^+$, neutrophils as Ly6G$^+$ and NK cells as
1174 NK1.1$^+$, using appropriate controls.
1175
1176
1177 ***Supplementary Figure 3: Gating strategy for IgG$_1$ and IgA producing plasma cells.***
1178 Organs were isolated to obtain single cell suspensions which were analysed by flow
1179 cytometry. Gating strategy involved removing doublets using FSC and SSC. Dead cells
1180 (positive for viability stain) were excluded. IgD$^+$CD3$^-$ cells were excluded by removing
1181 CD3$^+$ and IgD$^+$ cells from the analysis. IgG$_1^+$CD138$^+$ and IgA$^+$CD138$^+$ populations were
1182 identified using appropriate controls.
1183
1184 ***Supplementary Figure 4: IgG$_1^+$ cells in the granulomas of D7 bolus infected mice.***
1185 Serum was administered intravenously at D0, D2, D4, D6 to bolus infected animals.
1186 Formalin fixed paraffin embedded small intestine swiss rolls were obtained on D7 and
1187 co-stained with anti-mouse IgG$_1$ and DAPI. Top: mice who received trickle immune
1188 serum obtained from trickle infected mice. Bottom: mice who received non-immune
1189 control serum obtained from naïve animals. Experiment was performed once with 5
1190 mice per group, and representative images are presented. Scale bar=100µm.

Figure 1

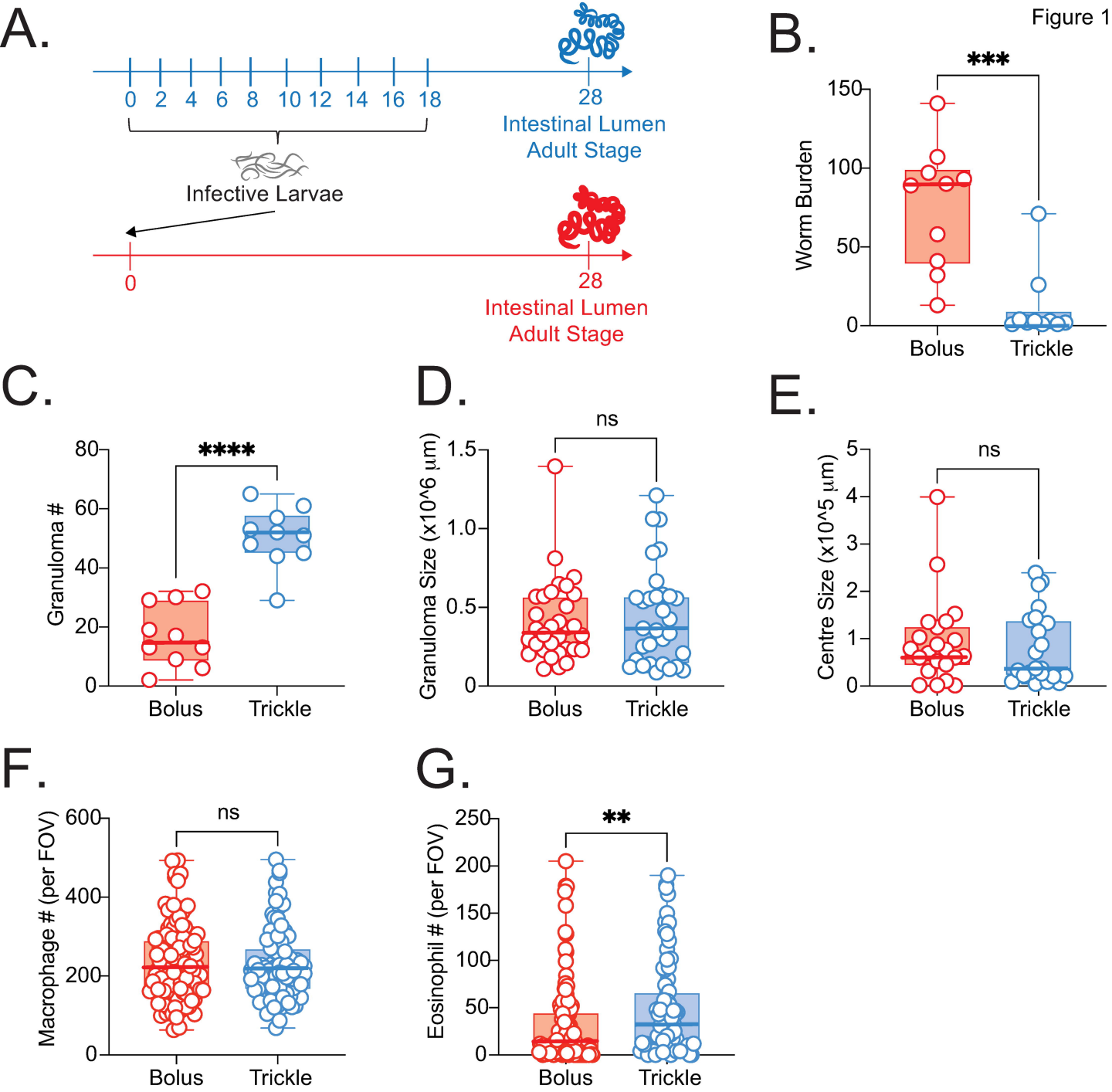
A.
0 2 4 6 8 10 12 14 16 18
28
Intestinal Lumen
Adult Stage
Infective Larvae
0
28
Intestinal Lumen
Adult Stage
B.
***
Worm Burden
150
100
50
0
Bolus
Trickle
C.
****
Granuloma #
80
60
40
20
0
Bolus
Trickle
D.
ns
Granuloma Size (x10^6 µm)
1.5
1.0
0.5
0
Bolus
Trickle
E.
ns
Centre Size (x10^5 µm)
5
4
3
2
1
0
Bolus
Trickle
F.
ns
Macrophage # (per FOV)
600
400
200
0
Bolus
Trickle
G.
**
Eosinophil # (per FOV)
250
200
150
100
50
0
Bolus
Trickle

Figure 2

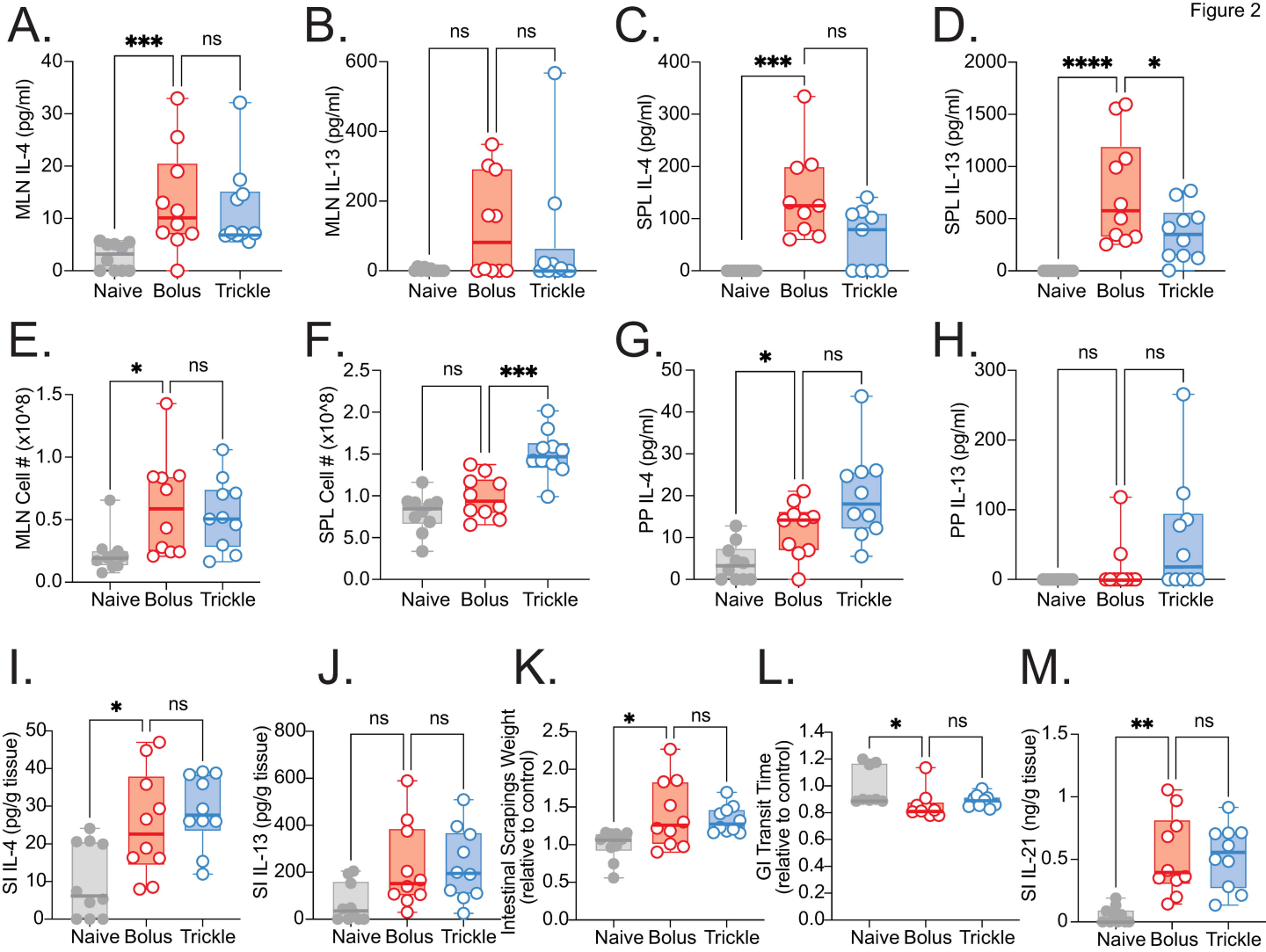
A.
MLN IL-4 (pg/ml)
***
ns
Naive Bolus Trickle
B.
MLN IL-13 (pg/ml)
ns
ns
Naive Bolus Trickle
C.
SPL IL-4 (pg/ml)
***
ns
Naive Bolus Trickle
D.
SPL IL-13 (pg/ml)
****
*
Naive Bolus Trickle
E.
MLN Cell # (x10^8)
*
ns
Naive Bolus Trickle
F.
SPL Cell # (x10^8)
ns
***
Naive Bolus Trickle
G.
PP IL-4 (pg/ml)
*
ns
Naive Bolus Trickle
H.
PP IL-13 (pg/ml)
ns
ns
Naive Bolus Trickle
I.
SI IL-4 (pg/g tissue)
*
ns
Naive Bolus Trickle
J.
SI IL-13 (pg/g tissue)
ns
ns
Naive Bolus Trickle
K.
Intestinal Scrapings Weight (relative to control)
*
ns
Naive Bolus Trickle
L.
GI Transit Time (relative to control)
*
ns
Naive Bolus Trickle
M.
SI IL-21 (ng/g tissue)
**
ns
Naive Bolus Trickle

Figure 3

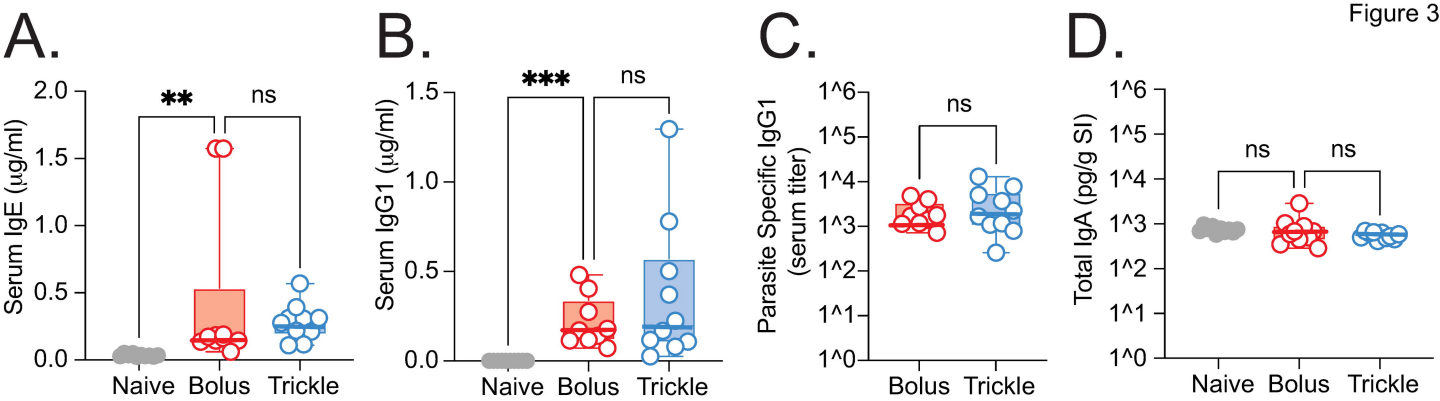
A.
Serum IgE (µg/ml)
2.0
1.5
1.0
0.5
0.0
**
ns
Naive
Bolus
Trickle
B.
Serum IgG1 (µg/ml)
1.5
1.0
0.5
0.0
***
ns
Naive
Bolus
Trickle
C.
Parasite Specific IgG1 (serum titer)
1^6
1^5
1^4
1^3
1^2
1^1
1^0
ns
Bolus
Trickle
D.
Total IgA (pg/g SI)
1^6
1^5
1^4
1^3
1^2
1^1
1^0
ns
ns
Naive
Bolus
Trickle

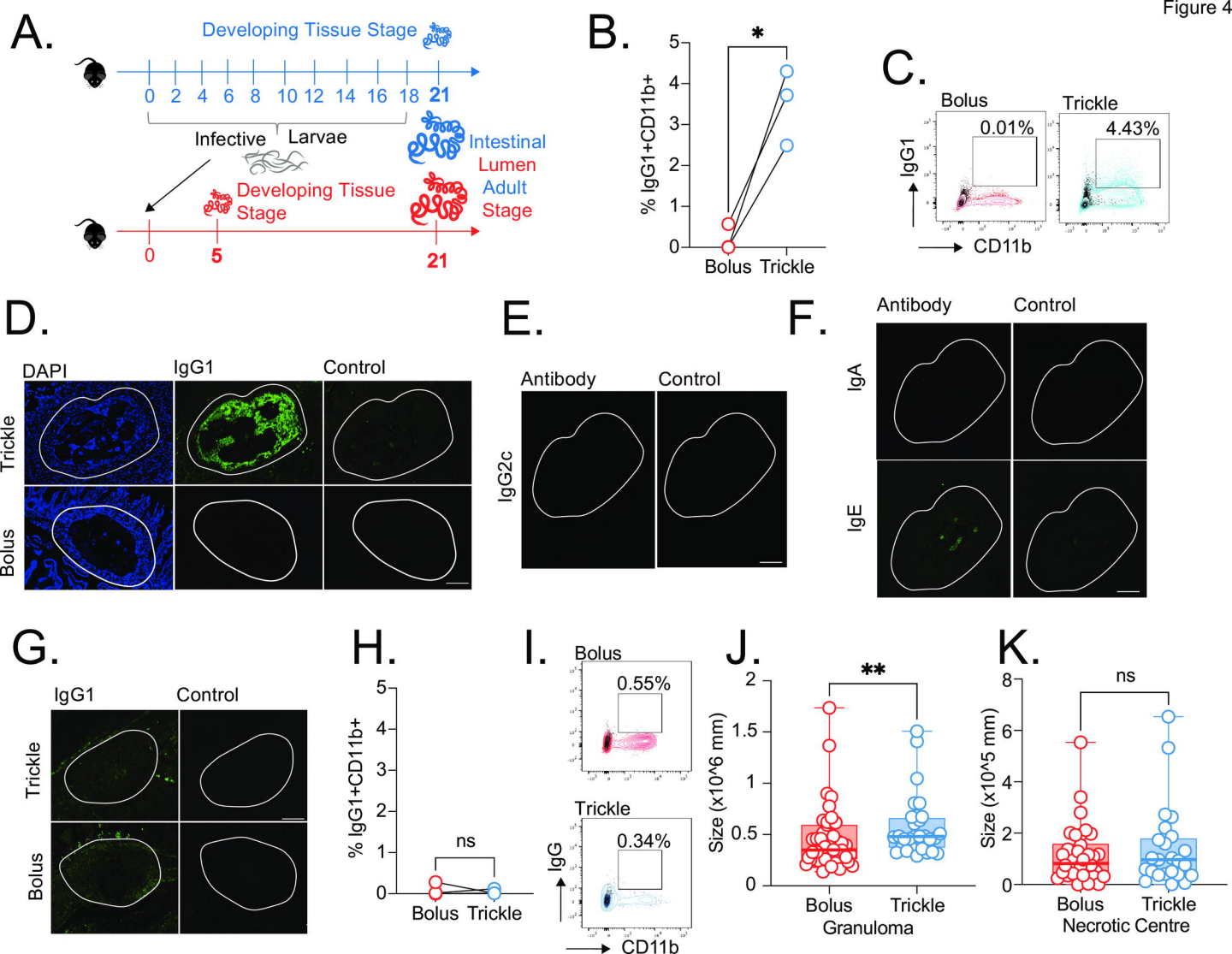
A.
Developing Tissue Stage
0 2 4 6 8 10 12 14 16 18 21
Infective Larvae
Intestinal Lumen Adult Stage
Developing Tissue Stage
0 5 21
B.
% IgG1+CD11b+
Bolus Trickle
C.
Bolus
Trickle
0.01%
4.43%
IgG1
CD11b
D.
DAPI
IgG1
Control
Trickle
Bolus
E.
Antibody
Control
IgG2c
F.
Antibody
Control
IgA
IgE
G.
IgG1
Control
Trickle
Bolus
H.
% IgG1+CD11b+
ns
Bolus Trickle
I.
Bolus
0.55%
Trickle
0.34%
IgG
CD11b
J.
Size (x10^6 mm)
Bolus Trickle
Granuloma
K.
Size (x10^5 mm)
ns
Bolus Trickle
Necrotic Centre

Figure 5

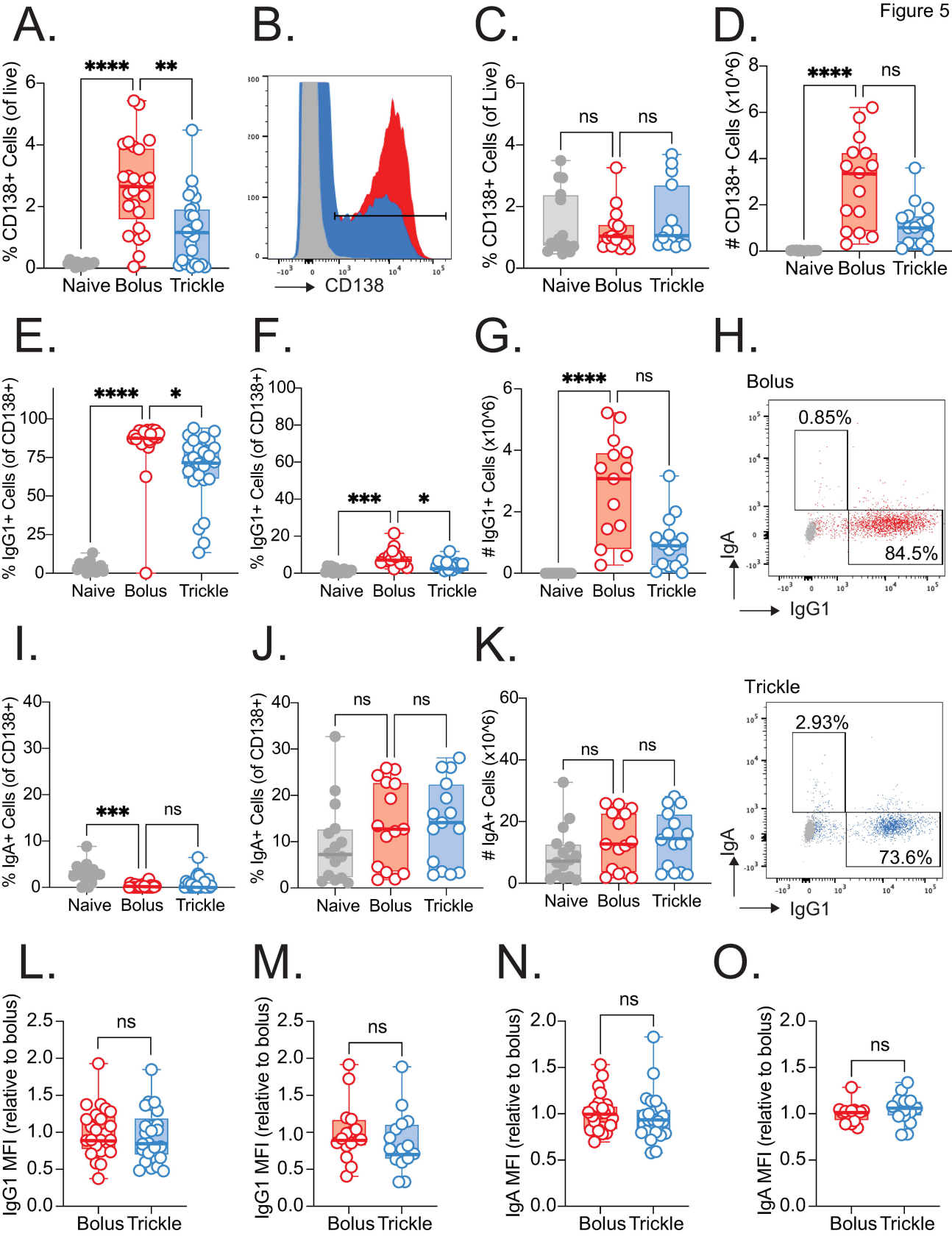
A.
% CD138+ Cells (of live)
****
**
Naive Bolus Trickle
B.
CD138
C.
% CD138+ Cells (of Live)
ns
ns
Naive Bolus Trickle
D.
CD138+ Cells (x10^6)
****
ns
Naive Bolus Trickle
E.
% IgG1+ Cells (of CD138+)
****
*
Naive Bolus Trickle
F.
% IgG1+ Cells (of CD138+)
***
*
Naive Bolus Trickle
G.
IgG1+ Cells (x10^6)
****
ns
Naive Bolus Trickle
H.
Bolus
0.85%
84.5%
IgA
IgG1
I.
% IgA+ Cells (of CD138+)
***
ns
Naive Bolus Trickle
J.
% IgA+ Cells (of CD138+)
ns
ns
Naive Bolus Trickle
K.
IgA+ Cells (x10^6)
ns
ns
Naive Bolus Trickle
Trickle
2.93%
73.6%
IgA
IgG1
L.
IgG1 MFI (relative to bolus)
ns
Bolus Trickle
M.
IgG1 MFI (relative to bolus)
ns
Bolus Trickle
N.
IgA MFI (relative to bolus)
ns
Bolus Trickle
O.
IgA MFI (relative to bolus)
ns
Bolus Trickle

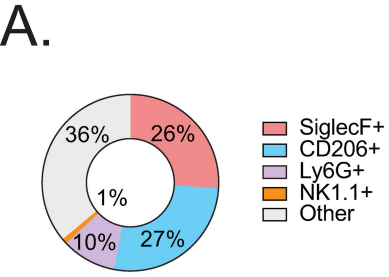
A.
36%
26%
1%
10%
27%
SiglecF+
CD206+
Ly6G+
NK1.1+
Other

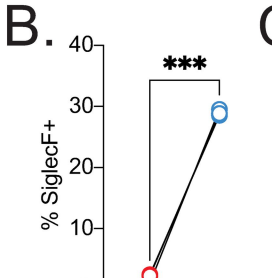
B.
***
% SiglecF+
40
30
20
10
0
Bolus
Trickle

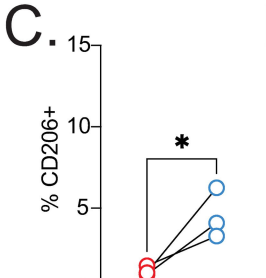
C.
*
% CD206+
15
10
5
0
Bolus
Trickle

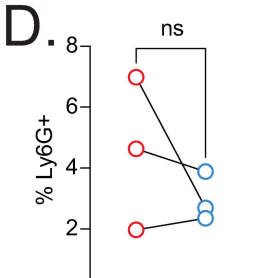
D.
ns
% Ly6G+
8
6
4
2
0
Bolus
Trickle

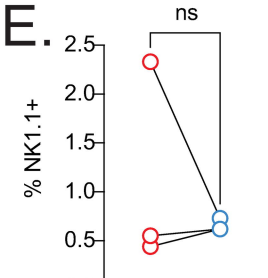
E.
ns
% NK1.1+
2.5
2.0
1.5
1.0
0.5
0.0
Bolus
Trickle

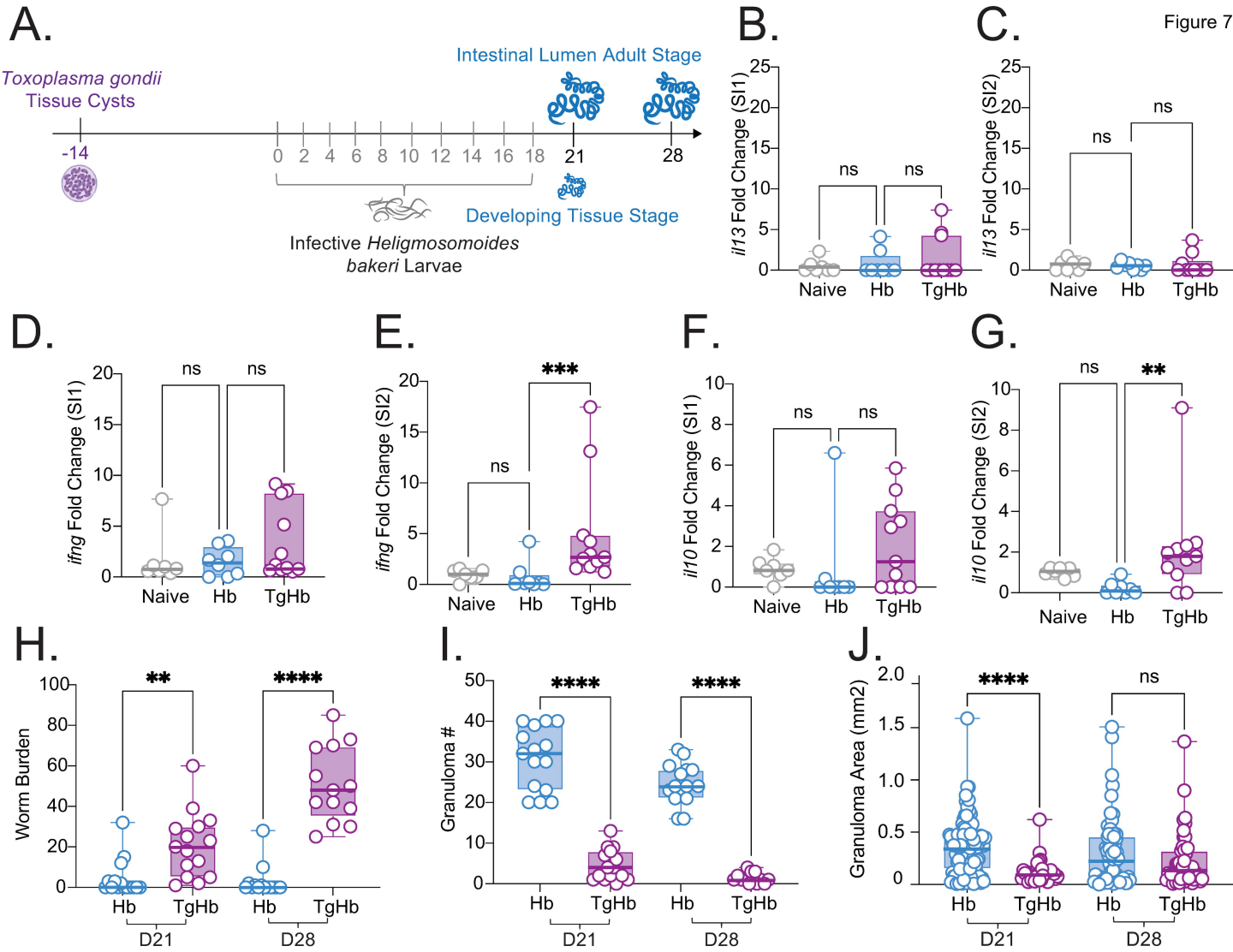
Figure 7
A.
Toxoplasma gondii
Tissue Cysts
Intestinal Lumen Adult Stage
-14
0 2 4 6 8 10 12 14 16 18
21
28
Developing Tissue Stage
Infective Heligmosomoides bakeri Larvae
B.
il13 Fold Change (SI1)
ns
ns
Naive
Hb
TgHb
C.
il13 Fold Change (SI2)
ns
ns
Naive
Hb
TgHb
D.
ifng Fold Change (SI1)
ns
ns
Naive
Hb
TgHb
E.
ifng Fold Change (SI2)
***
ns
Naive
Hb
TgHb
F.
il10 Fold Change (SI1)
ns
ns
Naive
Hb
TgHb
G.
il10 Fold Change (SI2)
ns
**
Naive
Hb
TgHb
H.
Worm Burden
**
****
Hb
TgHb
Hb
TgHb
D21
D28
I.
Granuloma #
****
****
Hb
TgHb
Hb
TgHb
D21
D28
J.
Granuloma Area (mm2)
****
ns
Hb
TgHb
Hb
TgHb
D21
D28

Figure 8

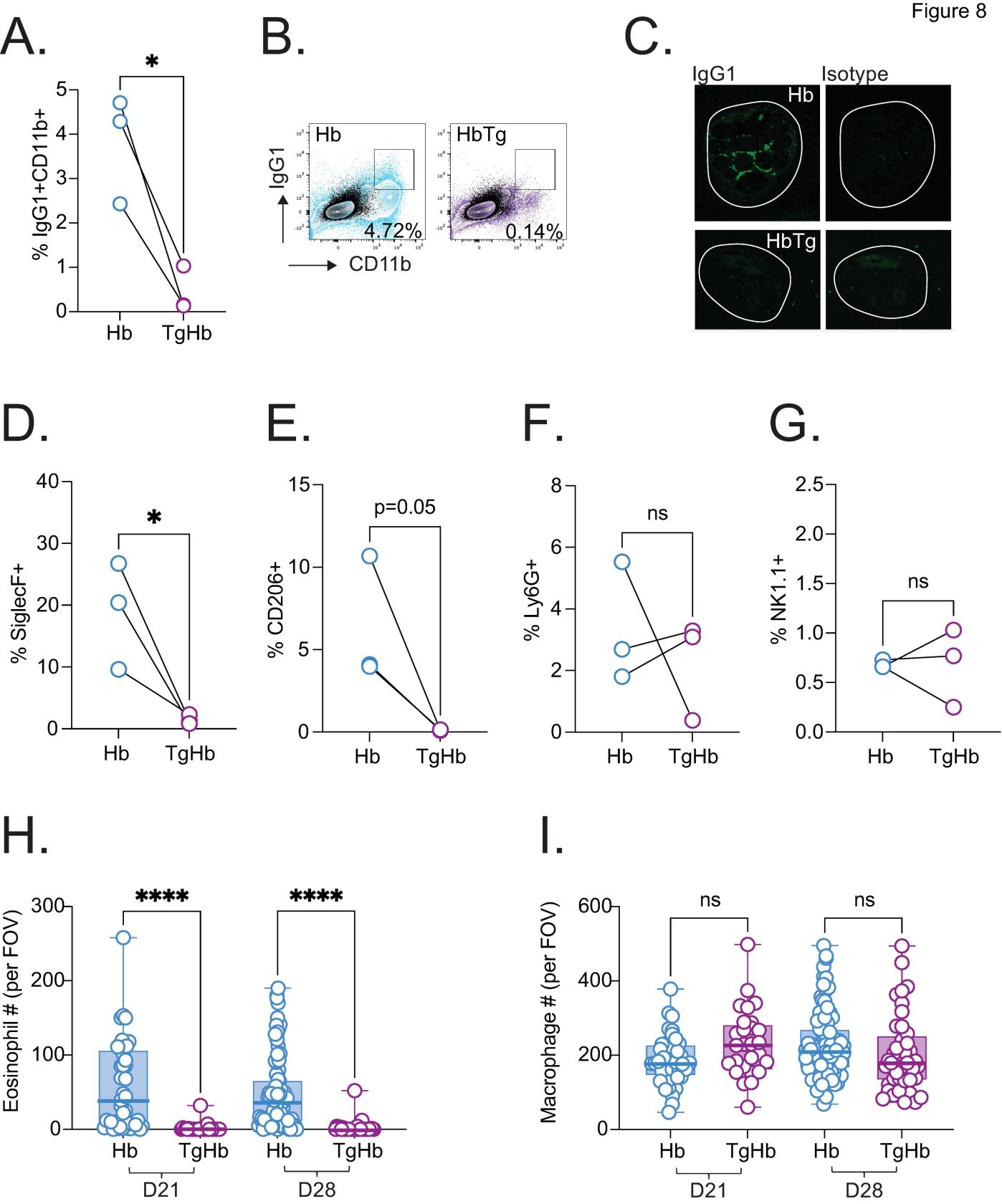
A.
*
% IgG1+CD11b+
5
4
3
2
1
0
Hb
TgHb
B.
Hb
HbTg
IgG1
CD11b
4.72%
0.14%
C.
IgG1
Isotype
Hb
HbTg
D.
*
% SiglecF+
40
30
20
10
0
Hb
TgHb
E.
p=0.05
% CD206+
15
10
5
0
Hb
TgHb
F.
ns
% Ly6G+
8
6
4
2
0
Hb
TgHb
G.
ns
% NK1.1+
2.5
2.0
1.5
1.0
0.5
0.0
Hb
TgHb
H.
****
****
Eosinophil # (per FOV)
300
200
100
0
Hb
TgHb
Hb
TgHb
D21
D28
I.
ns
ns
Macrophage # (per FOV)
600
400
200
0
Hb
TgHb
Hb
TgHb
D21
D28

Figure 9

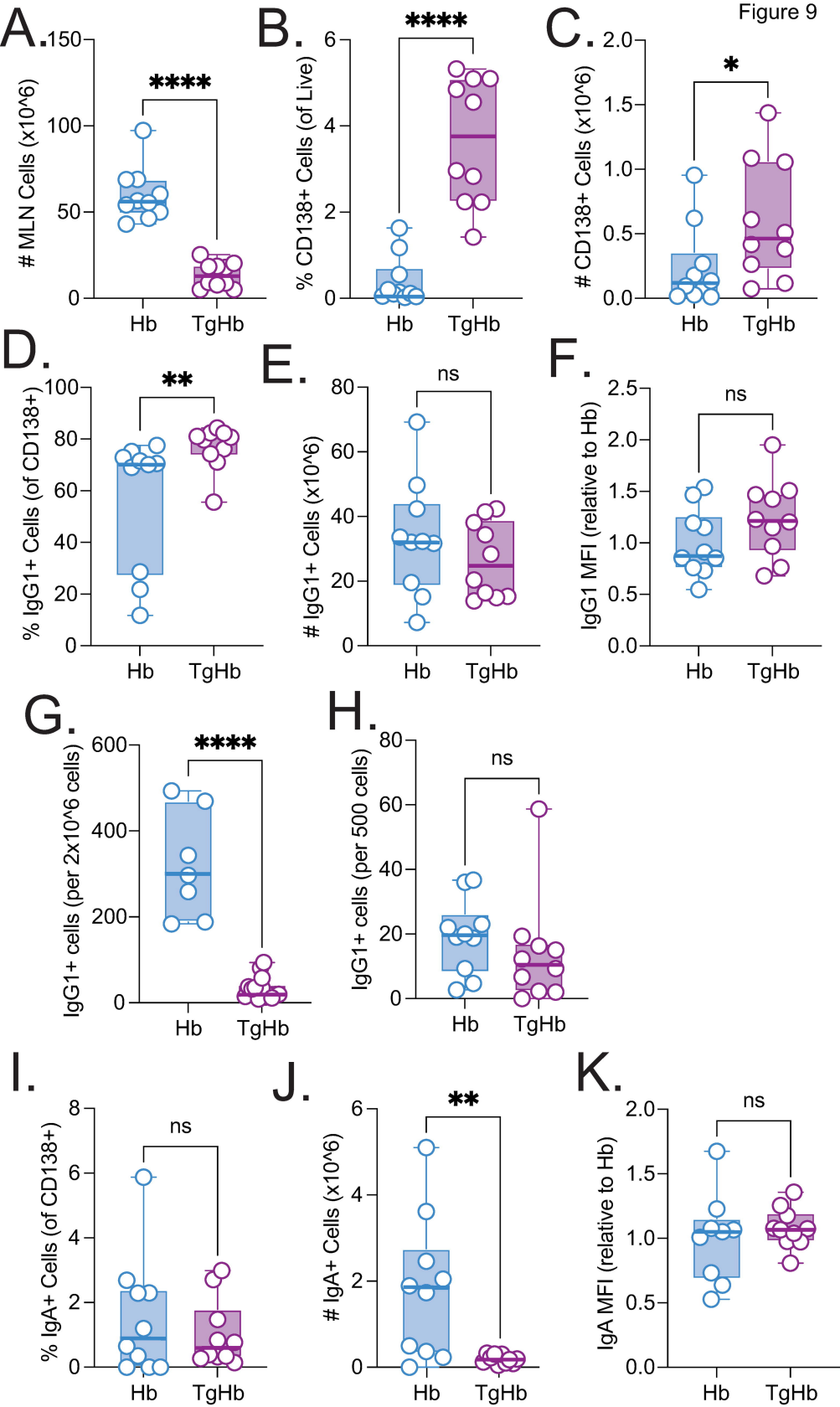
A.
MLN Cells (x10^6)
150
100
50
0
****
Hb
TgHb
B.
% CD138+ Cells (of Live)
6
4
2
0
****
Hb
TgHb
C.
CD138+ Cells (x10^6)
2.0
1.5
1.0
0.5
0.0
*
Hb
TgHb
D.
% IgG1+ Cells (of CD138+)
100
80
60
40
20
0
**
Hb
TgHb
E.
IgG1+ Cells (x10^6)
80
60
40
20
0
ns
Hb
TgHb
F.
IgG1 MFI (relative to Hb)
2.5
2.0
1.5
1.0
0.5
0.0
ns
Hb
TgHb
G.
IgG1+ cells (per 2x10^6 cells)
600
400
200
0
****
Hb
TgHb
H.
IgG1+ cells (per 500 cells)
80
60
40
20
0
ns
Hb
TgHb
I.
% IgA+ Cells (of CD138+)
8
6
4
2
0
ns
Hb
TgHb
J.
IgA+ Cells (x10^6)
6
4
2
0
**
Hb
TgHb
K.
IgA MFI (relative to Hb)
2.0
1.5
1.0
0.5
0.0
ns
Hb
TgHb